PARAMETRIC ANALYSIS OF A CONVERGENT-DIVERGENT NOZZLE FOR 2N COLD GAS PROPULSION OF A NANOSATELLITE

A Thesis Submitted to the

Department of Aerospace Engineering

INSTITUTE OF SPACE SCIENCE AND ENGINEERING

An Affiliate of

AFRICAN UNIVERSITY OF SCIENCE AND TECHNOLOGY

In Partial Fulfilment of the Requirements for the Degree of

MASTER OF SCIENCE

By

JEMILA JUMMAI IBRAHIM

(Reg, No. 440831)

SEPTEMBER, 2021

DEDICATION

I dedicate this thesis to Almighty Allah for giving me the strength, courage, knowledge, wisdom and good health to pursue this degree especially in the difficult times. This thesis is also dedicated to my parents, Engr. Dr H.D Ibrahim and Mrs. Mariam Ibrahim who have made everything possible to ensure that I have the best of education and provided a safe and enabling environments for me and my siblings.

CERTIFICATION

This is to certify that the thesis titled, "**PARAMETRIC ANALYSIS OF A CONVERGENT-DIVERGENT NOZZLE FOR 2N COLD GAS PROPULSION OF A NANOSATELLITE**", submitted to the school pf postgraduate studies, African University of Science and Technology (AUST), Abuja, Nigeria for the award of the Master's degree, is a record of original research carried out by Jemila Jummai Ibrahim in the Aerospace Department of the Institute of Space Science and Engineering (ISSE), affiliate of AUST.

PARAMETRIC ANALYSIS OF A CONVERGENT-DIVERGENT NOZZLE FOR A 2N COLD GAS PROPULSION SYSTEM OF A NANOSATELLITE

By

JEMILA JUMMAI IBRAHIM

A THESIS APPROVED BY THE DEPARTMENT OF AEROSPACE ENGINEERING

RECOMMENDED:

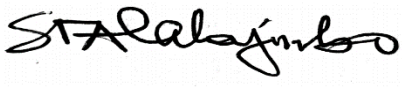

APPROVED:

ABSTRACT

In recent times, the concepts of microsatellite development have been a versatile subject ranging from their ability to reduce overall cost of satellites to their improved efficiency and adaptability. This has brought new innovations about creating micro-components for the satellite missions. The study of convergent-divergent (C-D) nozzle is an ever-growing research area due to its wide applications particularly in the aerospace field. Hence, this research study particularly looks into studying the influence of varying divergence angle and divergence length on flow parameters for optimum nozzle design.

Propellant selection criteria were drawn up for cold gaseous propellants to test their effectiveness leading to the choice of compressed air and Nitrogen as preferred propellants due to their availability, inertness and non-toxicity. Varying the divergence angle of a C-D nozzle produced a series of nozzle geometries and the analysis of simulation results yielded an optimum angle of 15° with choking effect at the throat located at 0.3m. Other divergence angles considered including 5°, 10°, 20°, 25° and 30^{o} generated multiple shocks across the nozzle throat. A divergence length of 1.35m produced the highest exit pressure of 61.756kPa close to ambient pressure. Divergence length of 1.35m coupled with a divergence angle of 15° appears to be most appropriate for the design of a C-D nozzle suitable for microsatellite propulsion system.

ACKNOWLEDGMENTS

I would like to thank Almighty Allah for providing me with an amazing opportunity, giving me patience when things became rough, good health and for seeing me through the length of the MSc program. I would like to express my gratitude to several individuals for supporting me throughout my Graduate study. I wish to express sincere gratitude to my parents; Engr. Dr HD Ibrahim and Mrs. Mariam Ibrahim for their support, effort and prayers that have given me strength and guidance when writing my Master thesis. I would like to show gratitude to my siblings; Ismaila, Umar, Ramatu and Chika for their amazing support.

I also wish to express gratitude to Professor Agboola for his continuous support, patience, helpful information, practical advice and guidance that have helped me to complete my thesis successfully. I would like to express my sincere thanks to the Institute of Space Science and Engineering (ISSE) and African University of Science and Technology (AUST) for accepting me into the MSC program and providing me with immense experience.

I am also grateful to my classmates, work colleagues and friends who have been of tremendous help during the course of my MSc.

Thanks for all your encouragement!

TABLE OF CONTENTS

LIST OF FIGURES

LIST OF TABLES

LIST OF ABBREVIATIONS

1D	One Dimensional
2D	Two dimensional
3D	Three Dimensional
AM	Additive Manufacturing
CAA	Clean Air Act
CAD	Computer Aided Design
CD	Converging – Diverging
CEA	Chemical Equilibrium Analysis
CFD	Computational Fluid Dynamics
CGP	Cold Gas Propulsion
DNS	Direct Numerical Simulations
EP	Electric Propulsion
EPA	Environmental Protection Agency
FDM	Finite Difference Method
FEM	Finite Element Method
FVM	Finite Volume Method
LEO	Low Earth Orbit
LES	Large Eddy Simulations
MSDS	Material Safety Data Sheet
NASA	The National Aeronautics and Space Administration
NASRDA	National Space Research and Development Agency
RANS	Reynolds Averaged Navier Stokes

NOMENCLATURE

A	Area, *m*
A_c	Convergence Area, m^2
γ	Ratio of specific heats
F	Thrust, *N*
V	Velocity, m^2/s
A_c	Chamber Area, m^2
A_e	Exit Area, m^2
A_t	Throat Area, m^2
I_{sp}	Specific Impulse, *s*
I_{sp}, m	Measured specific impulse, *s*
I_{sp}, t	Total specific impulse, *s*
C*	Characteristics Velocity, m^2/s
D_e	Exit Diameter, *m*
D_t	Throat Diameter, *m*
e	Energy
L_{cn}	Length of convergent nozzle, *m*
L_{dn}	Length of divergent nozzle, *m*
M	Mach Number
$\dot{m}$	Mass flowrate, *kg/s*

M_e	Exit Mach Number
m_f	Final mass, *kg*
m_i	Initial mass, *kg*
M_r	Molecular Weight
P_B	Back Pressure
P_{crit}	Critical Pressure
P_E	Exit Pressure
P_r	Regulator/ Chamber Pressure, *pascal*
Q	Volumetric flowrate, m^3/s
R	Gas Constant
r_c	Combustion radius, *m*
r_t	Throat radius,
r_e	Exit radius, *m*
T_b	Boiling Temperature
T_{cr}	Critical Temperature
T_m	Melting Temperature
T_o	Ambient Temperature, *K*
V_c	Chamber Velocity, m^2/s
V_e	Exit Velocity, m^2/s
β	Convergent angle
ρ	Density, kg/m^2
θ	Divergent angle
Φ	Dissipation term

ε	Expansion ratio
$\boldsymbol{\tau_{ij}}$	Viscous stress tensor

1.0 INTRODUCTION

Space travel has been a revolutionized concept with endless possibilities. The space industry in Nigeria is rapidly evolving with increase expert knowledge and the use of indigenous materials to develop space related products. There is a huge financial burden on large satellites into outer space hence the development of smaller, cost-effective satellites has now become a trending topic. The recent increase in demand and the technological advances related to small satellites have pushed the need to develop small subsystems components (Seubert et al., 2007), for instance the use of additive manufacturing (AM) in igniters, injectors and combustion chambers for their rocket engines ("3D Print. Sp.," 2014).

The productivity of a propulsion system is mostly affected by the nozzle performance. The function of a nozzle is to convert heat energy to kinetic energy by controlling the rate of flow, pressure and speed. A nozzle is required to change high pressure and temperature into high velocity, low temperature and pressure gases(Length et al., 2017). A nozzle typically has three different section- converging section, throat and divergent section. The smallest point where the diameter of the nozzle is called the throat. The converging section is the upstream section of the nozzle; the divergence section is known as the downstream section of the nozzle. As the nozzle profile goes from the pipe to the start of the throat, the area of the converging section decreases whereas the are diverging section profile increases for the end of the throat to the pipe (Singh et al., 2019). The performance of a nozzle is based on the critical pressure ratio and pressure drop across the nozzle. The critical pressure ratio is defined as the lowest ratio of downstream pressure to upstream pressure (Pc/Pe) when the flow is choked (M=1). A choked flow usually occurs when the Mach number is 1. An optimum nozzle geometry is achieved when the choked flow critical pressure ratio is large compared to other nozzle geometries.

Several research works have been carried out on the design, fluid flow and effect of various parameters on a nozzle. Previous studies have researched on the effect of an exit diameter on the performance of a converging- diverging annular nozzle. It was concluded that by reducing the exit diameter, there is an increase in velocity and decrease in pressure (Kundu et al., 2007). Another study investigated the effects of divergent angle variation on a C-D rocket engine nozzle; Raghu Ande concluded that an optimum Mach number is achieved at a divergent angle of 15° (Ande & Kumar Yerraboina, 2018). In an ideal design condition, the expansion ratio of the nozzle is chosen so that the exit pressure is the same as the ambient pressure to allow only a shear layer occur between the high-speed nozzle and the ambient. The ambient pressure at sea level is higher so that the nozzle flow is over expanded, and the speed of the flow slows down outside of the nozzle through a series of shocks. At high atmospheric altitudes, the flow can be under expanded and expansion waves deflect the flow out leading to a high bulge in the rocket plumes. In extreme cases, the shocks can enter the nozzle, resulting to poor performance (Dumitrescu et al., 2018).

This research study aims at investigating the influence of divergence angle and divergence length variation on some critical flow parameters for optimum design of a convergent-divergent nozzle while maintaining the same convergence section of the conical nozzle of a microsatellite propulsion system.

1.1 PROBLEM STATEMENT

Global research has shown an increment on the use of micro/nanosatellites in the aerospace industry. Nozzles are fast evolving and usually uniquely designed for specific missions. Studies on the nozzle design parameters can enhance the effectiveness of a cold gas propulsion system in a microsatellite. The use of a Computational Fluid Dynamics software such as ANSYS FLUENT can reduce cost, resources and aid in getting fast and efficient numerical results.

1.2 AIM AND OBJECTIVES

This research study is aimed at carrying out numerical experiments on a convergent-divergent nozzle for optimum thrust performance. The simulation results may find industrial applications in the manufacturing of a C-D nozzle suitable for microsatellite propulsion system.

The objectives of the research study are as follows:

- To identify a sustainable, non-reactive, inert gaseous propellant for the microsatellite propulsion system.
- To study the influence of varying the divergence angle on the design parameters of a C-D nozzle.
- To investigate the effect of divergence length variation on the flow parameters and overall thrust performance of a C-D nozzle.

1.3 RESEARCH QUESTIONS

As space propulsion is an ever-evolving area of research, some questions need to be considered in order to develop a well thorough investigation on the effects of changing a satellite nozzle parameter. From an engineering point of view, the following questions are posed:

- What is the optimum expansion ratio for a micro/nanosatellite?
- What are the ideal divergent angle and length suitable to produce a set amount of thrust?
- What are the available fabrication methods for nozzle manufacturing?
- Can the technology be scaled up?

These questions are a few of which this research intends to address.

1.4 SIGNIFICANCE OF STUDY

On completion, this research project will provide a possibility of a building block for future students. As it is a university project, students who are of interest in propulsion subsystem or any other subsystem can use the knowledge / further work from his project to develop a futuristic model. Intense and thorough investigation on nozzle parameter is a very important aspect in propulsion system, as it cuts down on excess cost in fabrication and testing.

1.5 SCOPE AND OUTLINE OF THESIS

The first step in the design of the propulsion system is a critical analysis of the propellants. A series of propellants is analyzed based on their thermodynamic properties, safety, environmental considerations and efficiency. These propellants range from industrial refrigerants to elemental gases. The next stage is the nozzle and tank design which are based on the physical properties of the chosen propellant. A computer aided design tool will be used to sketch the nozzle design. A Computational Fluid Dynamics software such as ANSYS Fluent will be used to validate the propellant fluid properties and propellant flow. The ambient pressure, ambient temperature, flow rate will be known, and a control volume will be created around the converging-diverging part of the nozzle. The preliminary section of the thesis is accompanied by five sections. A brief explanation of the chapters is given below:

2. Detailed Literature Review: This is a broad analysis of the three major components of this thesis (overview of satellites, propulsion system and use of a CFD software for nozzle design).

3. Methodology: The selection criteria used to define the basis for the cold gas propulsion system with its methodology and design procedure. It will include detailed analysis of the nozzle design. The parameters used in the design of the nozzle which are the foundation of the propulsion system. The methodology and Computational fluid analysis used in the evaluation of the propulsion system is presented.

4. Results and discussion: The results gotten from analytical calculations and the simulations are being analyzed against the literature review

5. Conclusion: The thesis concludes with a discussion of the overall propulsion system design and its approach in meeting up with the objectives of the thesis. A discussion of future work extending the scope of the project

2.0 LITERATURE REVIEW

2.1 MICROSATELLITE

Recent research and development activities in satellites have adopted the view of developing a smaller satellite with miniaturized components in order to reduce the design costs. A new survey shows how 60% of spacecraft costs have a direct correlation to the satellite operations (Nikolova, 2005). It is of high importance to reduce the cost of space operation through decreasing the mission cost especially for educational purposes. The idea of miniaturization has nurtured the interest of a growing demand for microsatellites. The major advantage of a microsatellite is its fast performance and relatively low production cost. Hence, it provides an excellent opportunity for the testing of new space subsystems in a limited time and low budget (Nikolova, 2005).

The word 'microsatellite' was derived by members of AMSAT-NA, a North America community. In the mid 1960's, they developed a spacecraft which had a weight below 10kg and was indeed micro at the time when considered with other well-known spacecraft missions. There are many ways to classify a satellite either by function, type of orbit, cost, size, performance, etc. Sweeting proposed the first known classification of satellites which is presented in Table 2-1 (Kramer & Cracknell, 2008)

Table 2-1: First satellite classification (Sweeting (1991) (Kramer & Cracknell, 2008)**)**

Nanosatellites	<10 kg
Microsatellites	10-100 kg
Minisatellites	100-500 kg
Small satellites	500-1000 kg
Large satellites	>1000 kg

2.2 PROPULSION SYSTEM

Propulsion systems are generally classified on the conversion of momentum to create thrust. The energy comes from either a chemical source or using an external energy source. Some propulsion systems do not contain any propellant at all. The propulsion performance is based on the total mass of the spacecraft and the propellant thrust (Kalsch I, 2000). A propulsion system is divided into photon, rocket and solar sail propulsion system. Rocket propulsion is further sub divided into thermal (chemical, solar, laser), Nuclear(radioisotope, explosion) and Electric (electrothermal, electromagnetic, electrostatic) (Lule & Lule, 2016)

2.2.1 THERMAL ROCKET PROPULSION

Chemical propulsion releases energy from a high-pressure combustion system of propellants usually a fuel and an oxidizing agent, subject the heating of reaction products to high temperatures (2500°C to 4100 °C). These gases are accelerated to high velocities and expelled through a nozzle. Liquid propellant is a form of chemical propulsion, liquids are fed under pressure from the chemical tanks to the thrust chamber. A monopropellant is a single liquid that contains both the oxidizing agent and the fuel. When catalyzed, it decomposes into hot gas. A bipropellant contains a liquid oxidizer and liquid fuel. In solid propellant, the propellant is usually contained in a combustion chamber. The solid propellant is known as grain, and it consists of all the chemical elements for complete combustion. Gaseous propellants typically use a high-pressured gas such as air, nitrogen or helium as their propellants. Hybrid propellants are a mixture of both liquid and solid propellant (Corradini et al., 2016).

Solar sail propulsion utilizes sunlight to accelerates vehicles through space. The device uses solar photons which are reflected off using reflective mirrors to create a photonic pressure that provides enough thrust (Murphy & Trautt, 2007). Laser Propulsion is an example of beam powered

propulsion; the energy source is a ground based (remote) laser system and its separate from the reaction mass. In chemical propulsion, the energy and reaction mass comes from the liquid or solid on the vehicle (Salgado et al., 2018).

2.2.2 NUCLEAR ROCKET PROPULSION

Nuclear Rocket Propulsion uses propellants (liquid hydrogen) to move around the nuclear core absorbing thermal energy. Thermodynamic expansion occurs through a nozzle producing high thrust and specific impulse (FAA, 2017). There are three forms of nuclear energy sources which are: fission reactor, radioactive isotope decay and fusion reactor. These forms get their energy within the nuclei of atoms. There are an extension of liquid propellant rockets (Sutton & Biblarz, 2010).

In nuclear fission reactor rocket, the heat is made by the fission of uranium in solid reactor material which is then transferred to the working fluid. These rockets typically have high thrust engines (>40,000N) with specific impulse values of 900s (Sutton & Biblarz, 2010).

Isotope decay engines is based on a radioactive material giving off radiation which is converted to heat. The temperature of the working fluid is raised based on the heat from the radioactive material. It produces low thrust and lower temperatures compared to other nuclear rockets. The last method is the Fusion method which creates nuclear energy that can heat a working fluid. There are currently concepts that have been studied under fusion engines but none have tested them (Sutton & Biblarz, 2010).

2.2.3 ELECTRIC ROCKET PROPULSION

Electric Propulsion (EP) based its electric power on external sources such as nuclear, solar radiation, receivers or batteries. The thrusters for electric propulsion uses ionized gases as the

propellant(Lule & Lule, 2016). Electric thrusters do not pose a limit on the propellant exhaust velocity and the mass of the propellant can be low. The thrust generated can be independent from the mass flowrate provided there is enough power. The basic concept of EP is the use of electrical energy to accelerate ionized propellants that delivers a high specific impulse (Levchenko et al., 2018). EP can be further classified into electrothermal, electrostatic and electromagnetic systems.

Electrothermal Propulsion is a combination of chemical and electric system; the propellant is heated electrically, and the hot gas is thermodynamically expanded and accelerated at supersonic velocity through a nozzle. They typically have thrust values ranging from 0.01 to 0.5N with exhaust velocities of 1000 to 5000 m/s. Commonly used propellants for electrothermal propulsion are hydrogen, helium, ammonia and nitrogen (Sutton & Biblarz, 2010). Resistojets are electrothermal propulsion devices that involves the heating of propellant through a resistively heated chamber before entering the nozzle. Arcjet is an example of a electrothermal propulsion device that involves the heating of propellant through a high current arc line with the nozzle feed system (Goebel & Katz, 2008).

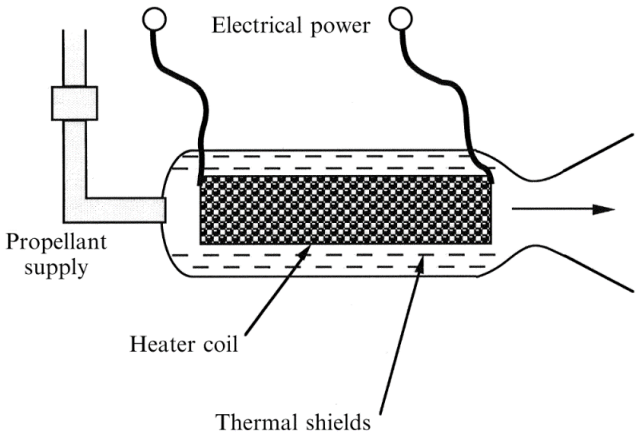

Figure 2-1: Schematics of an Electrothermal Propulsion System (Turner, 2008)

Electrostatic propulsion can also be known as ion propulsion. This type of propulsion involves the ionization of a working fluid such as xenon, which is electrically charged and accelerated at a very high velocity (usually 2000 to 60000m/s). The ions are then neutralized electrically and are combined with electrons to avoid buildup of a space charge on the vehicle (Sutton & Biblarz, 2010). Hall Thruster is a type of electrostatic propulsion device that uses a cross field discharge described by the Hall effect to create the plasma. Hall thruster specific impulse and efficiency is lesser than ion thrusters but the thrust at a set power is higher. Electrospray and Field Emission electric propulsion thruster are examples of electrostatic device which produces very low thrust (<1 mN) (Goebel & Katz, 2008).

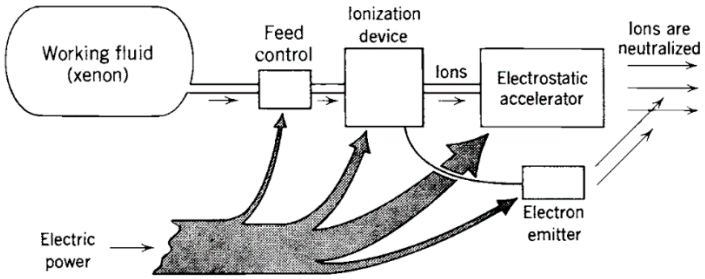

Figure 2-2: Schematics of an Electrostatic Propulsion System(Sutton & Biblarz, 2010)

Electromagnetic Propulsion is a process where ionized propellants are accelerated by interactions of external and internal magnetic fields with the flow of electric currents through the stream(Jahn & Lyman, 1969). Pulsed plasma thruster is an electromagnetic thruster that uses a pulsed discharge to ionize an amount of solid propellant evaporated into a plasma arc and electromagnetic effect in the pulse to move the ions to high exit velocity. Magneto plasma dynamic thrusters are electromagnetic devices that utilizes high current arc to ionize a fraction of the propellant and electromagnetic forces (such as Lorentz forces) in the plasma discharge to speed up the charged

propellants (Goebel & Katz, 2008). Table 2-2 shown below illustrates a summary of the propulsion systems with the characteristics.

Table 2-1: Comparison of common propulsion systems (Aysu, 2019)

Propulsion Technology	Orbit Insertion		Orbit Maintenance and Maneuvering	Attitude Control	Typical I_{sp} (s)
	Perigee	Apogee			
Cold gas			Yes	Yes	30-70
Solid	Yes	Yes			280-300
Monopropellant			Yes	Yes	220-240
Bipropellant	Yes	Yes	Yes	Yes	305-310
Dual Mode	Yes	Yes	Yes	Yes	313-322
Hybrid	Yes	Yes	Yes		250-340
Electric		Yes	Yes		300-3000

The specific impulse of a system is defined as a measure of a propulsion system's efficiency. It is usually measured in seconds.

2.2.4 COLD GAS PRINCIPLES

Cold gas propulsion (CGP) system will be the ideal propellant for this research. Cold gas systems are the safest and simplest method currently in use especially for small satellites. The gas is stored under pressure in a tank and expelled as a cold propellant through a nozzle. The thrust is usually low with low efficiency (Krejci & Lozano, 2018). A cold gas system usually consists of a gas tank, propellant feed, pressure regulator, drain/relief/ solenoid valve and the nozzle.

Cold gas propulsion systems typically rely on ejecting compressed liquid/ gaseous propellants to generate thrust. In a CGP system, there is no combustion hence the system only requires one propellant and can be designed with little or no complexity (Tummala & Dutta, 2017). Figure 2-3 represents a schematic of a CGP system.

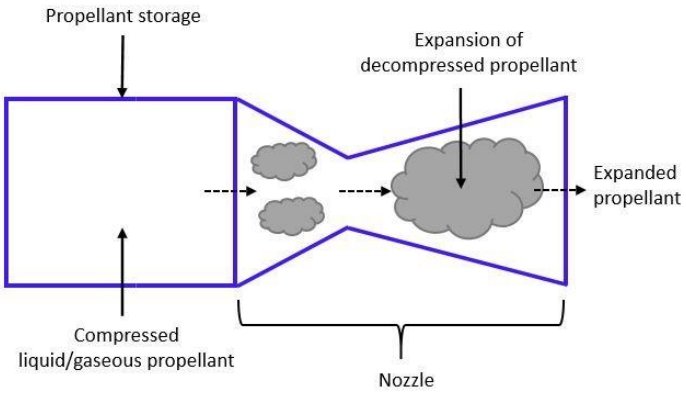

Figure 2-3: Schematics of a Cold gas Propulsion System (Tummala & Dutta, 2017)

The thrust in a CGP system is directly proportional to the pressure of the propellants in the propellant storage tank and as time increases, the propellant tank pressure decreases leading to a decrease in the initial thrust of the system (Tummala & Dutta, 2017).

The specific impulse of a CGP system depends on the exit pressure to chamber pressure ratio also known as the pressure ratio (P_e/P_c) and the characteristics velocity (C*). The specific impulse relationship is expressed as

$$I_{sp} = \frac{\gamma C^*}{g_o}\sqrt{\frac{2}{\gamma-1}\left(\frac{2}{\gamma+1}\right)^{\frac{\gamma+1}{\gamma-1}}\left(1-\frac{P_e}{P_c}\right)^{\frac{\gamma-1}{\gamma}}} \qquad (2.1)$$

where γ is the ratio of specific heat at constant pressure and volume, g_o is gravity at sea level.

The pressure ratio relates to the expansion of the propellant. The characteristics velocity of any CGP system is a function of the velocity of propellants in Mach number(Tummala & Dutta, 2017). C* can also be used in comparing the performance of different chemical rocket propulsion systems and propellants (Sutton & Biblarz, 2010) and can be represented as:

$$C^* = \sqrt{\frac{2\gamma}{\gamma+1}}\, RT_0 \qquad (2.2)$$

where R is the ideal gas constant, T_0 is the ambient temperature.

2.2.5 TANK DESIGN

The propellant tank design is the most important part of the research because it involves the foundation of the numerical experiment. When designing a propulsion system, the laws of conservation of momentum is required to allow the spacecraft to impart momentum. The generalized equation is listed below:

$$\dot{\boldsymbol{P}} = \sum F + \sum \dot{m}v \qquad (2.3)$$

This is simply stated in words as the time rate of change in momentum of any system is equal to the total sum of all the forces acting on a system plus the total sum of the mass fluxes times their velocities into the system (Roddy, 2020). The ΔV is an important merit of figure for a propulsion system as it shows the amount of velocity change and thrust the system can release. The ΔV will have to be optimized on the mission needs and the tradeoffs between the ΔV and thrust needs to be considered. The Tsiokwoski equations or rocket equation shows a relationship between the mass of propellant, mass of spacecraft the specific impulse of the propulsion system on how the ΔV can be achieved. This relationship can be seen in the equation below:

$$\Delta V = g I_{sp} ln\left({m_i}/{m_f}\right) \qquad (2.4)$$

where m_i is the initial mass of propellant and m_f is the final mass of propellant.

Satellite propellants tanks used in propulsion can either be spherical or cylindrical in shape. The weights of the tankas are a result of the structural design of the tanks (Anis, 2012). Tank Sizing is an important parameter in the system design, which requires foundation of thermodynamics and fluid flow. The volume of the gas tank is determined by its given mass and density at an ambient temperature of 298 K.

2.2.6 NOZZLE DESIGN

A nozzle is typically used to control the expansion of gases from high pressure to low pressure and moves the combustion products to high exit velocities. By using the concepts of Newton's Third Law, a relative motion is created when matter is ejected out of a nozzle, hence producing and opposite force that is applied There are three types of nozzles normally used in the space industry which includes diverging, converging and converging-diverging (Croteau, 2018).

The convergent- divergent (C-D) nozzle also known as de-Laval nozzle can convert subsonic flow in a converging area to supersonic flow in the diverging area while preventing shock in the flow (Tan et al., 2019). The nozzle shape aids the movement of a high pressure, low velocity gas that enters the nozzle and its compressed as it reaches the smallest diameter section, where the gas velocity increases to the speed of sound (Anis, 2012)

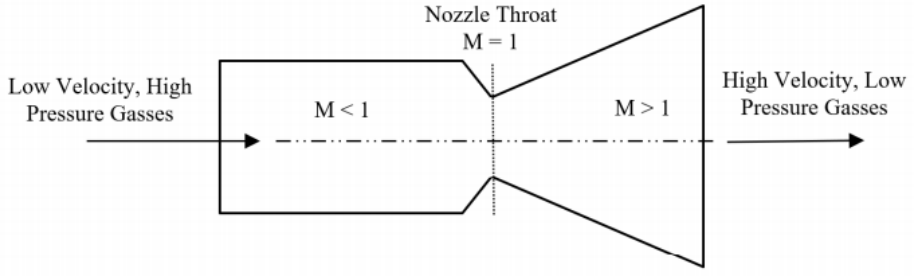

Figure 2-4: Converging- Diverging Nozzle Concept (Anis, 2012)

Supersonic nozzles create a high velocity effect with a Mach number greater than 1, these are necessary when designing as it achieves the necessary conversion of thermal energy to kinetic energy to creates maximum thrust. The three main types of supersonic nozzles include conical, bell and plug nozzles. Conical nozzles have a cone like shape with a constant expansion rate. One of the major advantages is the ease to manufacture compared to the bell concept. The bell nozzle also known as annular nozzle has a curved expansion contour which allows for a highly efficient conversion of thermal energy to kinetic energy. The nozzle tends to be shorter and lighter compared to the conical nozzle. The size makes it difficult to manufacture hence high manufacturing cost. Bell/ annular nozzle has different variations hence its selection is based on the type of application. Bell and conical supersonic nozzles reach maximum thrust at a designed altitude which is at an optimized altitude during flight. Plug nozzles has a feature where the fluid and wall contour are being accelerated around the expansion point. They can adjust to the altitude during flight allowing for maximum thrust throughout the rocket trajectory. This type of nozzle is less efficient for the conversion of thermal energy to kinetic energy due to the flow being restricted at one side by a constant pressure boundary. An aerospike nozzle is a typical example of a plug nozzle (Denton & Denton, 2008). Figure 2-4 illustrates the shape and size of the different supersonic nozzles. This project will focus on using a conical converging and diverging nozzle due to its low manufacturing cost, weight and ease of use applications.

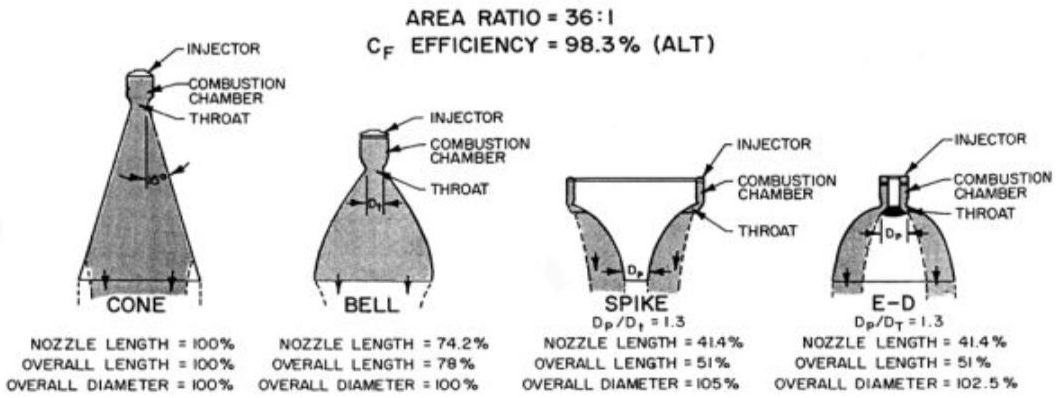

Figure 2-4:Nozzle Profiles (Denton & Denton, 2008)

A typical design of nozzle consists of the throat dimeter (D_t), axial length of the nozzle from the throat to the exit plane Ln, expansion ratio ε (using area), initial wall angle of the parabola n and the nozzle exit wall angle e (Tan et al., 2019). In designing a conical nozzle, the fluid properties change in the flow field is not considered. It is mainly calculated from geometry and exit area to throat area ratio (area ratio) for a desired exit Mach number. The area ratio equations assume the fluid flow is inviscid, irrotational, isentropic and is based on the exit Mach number and the specific heats of the working fluid. The C-D nozzle design follows Newton second law which is given as:

$$F = \dot{m}V_e \tag{2.5}$$

where F is the force, $\dot{m}$ is the mass flowrate and V_e is the velocity at the exit. This can also be represented in terms of exit area (A_e) and the exit pressure (P_e) which can be seen as:

$$F = A_e\, P_e \tag{2.6}$$

For satellites, the thrusters are designed for infinite expansion (vacuum conditions) where the ambient pressure is zero. The thrust equation becomes:

$$F = A_t P_c \gamma \left[\left(\frac{2}{\gamma-1}\right)\left(\frac{2}{\gamma+1}\right)\left(1-\frac{P_e}{P_c}\right)\right] + P_e A_e \quad (2.7)$$

where A_t is the throat area,

The area and pressure ratios are given as:

$$\varepsilon = \frac{A_e}{A_t} = \frac{1}{M_e}\left\{\left(\frac{2}{\gamma+1}\right)\left(1+\frac{\gamma-1}{2}{M_e}^2\right)\right\}^{\frac{\gamma+1}{2\gamma-1}} = \frac{\pi.\, r_e^2}{\pi.\, r_t^2} \quad (2.8)$$

$$\frac{P_e}{P_t} = \left\{\left(1+\frac{\gamma-1}{2}{M_e}^2\right)\right\}^{\frac{\gamma}{\gamma-1}} \quad (2.9)$$

There are six nozzle parameter output that describes the efficiency and performance of a nozzle in a spacecraft. These parameters are mass flow rates, thrust, specific impulse, exit velocity and the change of velocity. The mass flow rate of the fluid can be seen as:

$$\dot{m} = \rho V_e A_e \quad (2.10)$$

where $\dot{m}$ is the mass flow rate, ρ is the density of the working fluid. Specific impulse mathematical expression is:

$$I_{sp} = \frac{F_T}{\dot{m}g} \quad (2.11)$$

where Isp is the specific impulse, F_T is the thrust and g is the gravitational constant at sea level which has a value of 9.80665 m/s^2 and 8.14 m/s^2 at LEO.

In the exit velocity (V_e) shown below, Q represent the volumetric flow rate and D_e is the exit diameter.

$$V_e = \frac{4Q}{\pi {D_e}^2} \quad (2.12)$$

The change in velocity can be expressed as:

$$\Delta V = V_{eq} \ln\left(\frac{m_f}{m_e}\right) = I_{sp} g ln\left(\frac{m_f}{m_e}\right) \quad (2.13)$$

where ΔV is the change in velocity, V_{eq} represent the equivalent velocity.

From a ΔV standpoint, it is of high advantage to have a high area ratio that results to a small throat area and diameter (Seubert et al., 2007). The final parameter is the Mach number. The Mach number can be mathematical expression as:

$$M = \frac{V_e}{C} \quad (2.14)$$

Where C is the speed of sound in dry air and its temperature dependent.

The expansion ratio of nozzles should be less than 15 at sea level conditions and a range of 20-400 for vacuum conditions ay optimum performance. A conventional nozzle has a semi divergent angle of 15° but at micro level, the semi divergent angle is said to increase to 28° (Ranjan et al., 2018). Although studies show a divergent angle of less than 30°, an optimum divergent angle is still a critical aspect in converging-diverging nozzle design. Flow separation occurs when the boundary layer moves far enough against a hostile pressure gradient, where the speed of the boundary layer falls almost to zero and the fluid detaches from the surface of the object. In nozzle design, this occurs when the fluid moves towards the divergent section from the throat. The flow separation increases with the increase of the divergent angle and vice versa. The increase in the length of the divergent part will decrease the nozzle angle (Ahmer et al., 2014).

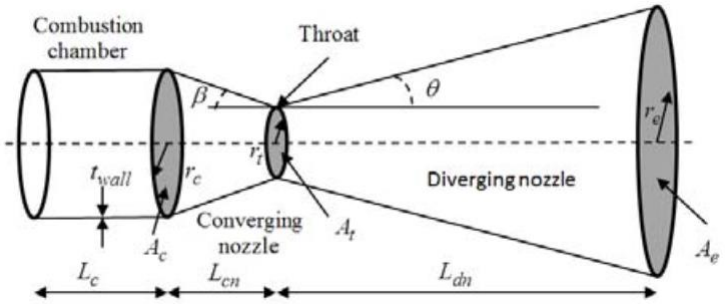

Figure 2-5: Detailed Schematics of a Convergent-Divergent Nozzle (Belega & Duc Nguyen, 2015)

To calculate the convergence area, combustion radius, divergent nozzle length and convergence nozzle length; the following equations are used:

$$A_c = 3A_t \tag{2.15}$$

$$r_c = \sqrt{\frac{A_c}{\pi}} \tag{2.16}$$

$$L_{dn} = \sqrt{\frac{A_e}{\pi}} . \frac{1}{\tan\theta} \tag{2.17}$$

$$L_{cn} = \sqrt{\frac{A_c}{\pi}} . \frac{1}{\tan\beta} \tag{2.18}$$

where A_c is the convergence area, r_c is the combustion radius, L_{dn} is the length of the divergent nozzle, L_{cn} is the length of the convergent nozzle, θ is the divergent angle and β is the convergent angle.

In real cases, losses at the convergent section exist hence the Mach number of 1 is not attainable at the throat. Due to the losses, the nozzle efficiency is assumed to be 0.90. It is assumed that the expansion of the fluid occurs adiabatically (no loss or gain of heat) but the expansion process is

never isentropic because of the irreversibility. A high divergent angle will lead to a high flow separation which leads to high losses. (Ahmer et al., 2014).

2.3 PRESSURE DISTRIBUTION IN A NOZZLE

A nozzle usually draws air from a storage tank with a constant stagnation pressure. The back pressure is assumed to be at the end of the diverging section as such air reaches sonic conditions at the throat. Mach number increases in the diverging section. Different area ratios give different Mach numbers. There are typically seven cases in a pressure velocity distribution scenario where the exit pressure of the nozzle is denoted as P_E and the back pressure is denoted as P_B.

Case 1 (No flow): When the valve is closed, there is no flow through the nozzle hence the pressure is constant at P_0. At this point, the Back pressure is equal to the exit pressure (P_B=P_E).

Case 2 (Isentropic subsonic flow): Opening the valve leads to changes in the distribution of pressure where $P_0 > P_B > P_{crit}$ (P_{crit} represent the critical pressure). The flow remains subsonic throughout the nozzle. The flow increases at the converging section and reaches its maximum at the throat. as the flow continues to accelerate to the diverging section, the gain in the velocity is reduced. The pressure decreases in the converging section reaches a minimum pressure at the throat and increases at the diverging section.

Case 3 (Choked Isentropic subsonic and supersonic flow): The back pressure is reduced to make the flow reach sonic conditions at the throat; $P_B = P_{crit}$. The throat pressure becomes P*. Subsonic flow still occurs at the diverging section as the back pressure is still high. The flow in the converging section is unchanged as the back pressure is further reduced.

Case 4 (Normal shock in the nozzle): A sudden change in the pressure occurs between the throat and the exit which is typically known as normal shock. In this case $P_{crit} > P_B > P_E$, the fluid at sonic veocity at the throat moves to supersonic velocity at the diverging section as the pressure decreases. The shock causes a drop in the velocity leading to subsonic conditions and an increase in pressure. Flow through the shock is mostly irresversible and cannot be classified as isentropic. As the back pressure decreases, the normal shock moves away from the throat and it reaches the nozzle exit as P_B approaches P_E. When $P_B = P_E$, the normal shocks occurs at the nozzle exit. The velocity of the fluid reduces to subsonic conditions as it cosses the normal shock at the end of the nozzle and the flow is supersonic throughout the diverging section.

Case 5 (Normal shock at nozzle exit): The back pressure keeps decreasing till it reaches a limiting case of Navier Stokes equation at the nozzle exit. The shock waves in the divergent section moves to the exit plane. The pressure increases outside the nozzle plane and therefore the exit plane pressure and the back pressure are the same ($P_E = P_0$). Entropy increases outside a shock.

Case 6 (Overexpansion): In this case the back pressure is drastically reduced leading to a subsonic flow through out the converging section of the nozzle. It is sonic at the throat and supersonic at the divergent section. An overexpanded flow means theexit pressure is lower than the gaseous pressure which typically occurs in this case leading to a contraction once it exits the nozzle. The contractions causes a non-isentropic oblique pressure waves.

Case 7 (Design Condition): A nozzle is typically designed to have the back pressure low enough to match the pressure of the supersonic flow at the exit. The creates an isentropic flow in the nozzle and downstream. This is the most efficient case for nozzle design.

Case 8 (Underexpansion): In this case the back pressure is now lower than the exit pressure of the supersonic flow compared to the overexpansion case. The exit flow must expand to equal the reserboir pressure and the flow is governed by oblique pressure waves [(Blog, n.d.),(Mzad & Elguerri, 2012),(William J Devenport, n.d.)].

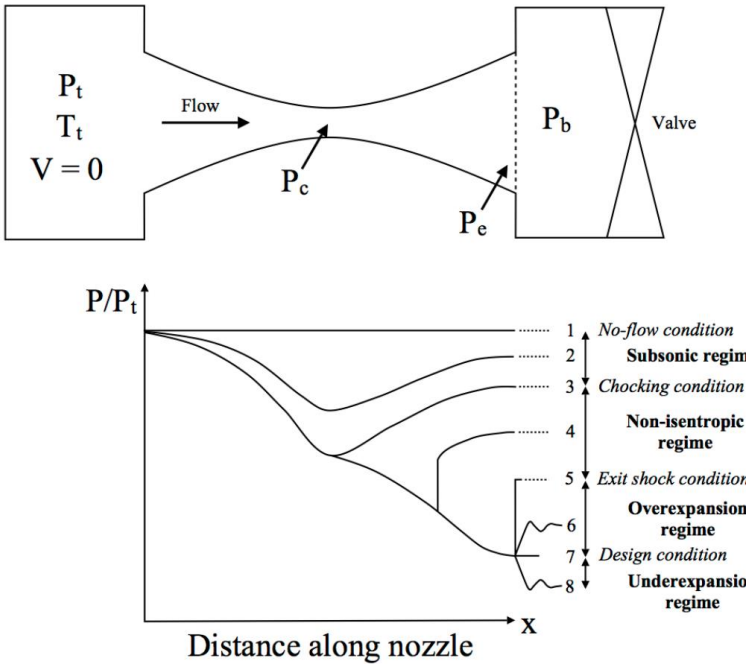

Figure 2-6: Variations Of Pressure Along The Length Of A Convergent And Divergent Nozzle (Blog, n.d.)

2.4 COMPUTATIONAL FLUID DYNAMICS (CFD)

Numerical analysis is done to assess the propulsion system performance before fabrication and testing. The use of fluid flow analysis with the aid of computational fluid dynamic (CFD) is important for solving problems that involve flow of fluids, heat transfer, mass transfer and chemical reactions (Lin et al., 2020). CFD allows the designer to spot any changes in the flow such as shocks or changes in the thermophysical properties of the fluid.

The governing equations are the lifeline of CFD. These equations are known as the Navier Stokes (NS) equations and were discovered 150 years ago by a French Engineer called Claude Navier and an Irish Mathematician - George Stokes. CFD is an application-based supercomputing used to solve the famous equation. The equations are based on the assumption that a fluid particle can deform under shear stress. The continuity, momentum and energy equations are the cornerstones of any CFD program and constitute as the Navier Stokes equation.

The continuity equation says that the mass is conserved, it is also known as the conservation of mass. The continuity equation can be written as

$$\frac{\partial p}{\partial t} + \nabla.\left(\rho \vec{U}\right) = 0 \tag{2.19}$$

where $U = [u, v, w]$

The momentum equation is based on Newton's second law of motion that states F = ma, where m represents the mass of the particle and a is the acceleration. The momentum equation is written as:

$$\rho \frac{D\boldsymbol{V}}{Dt} = \nabla \tau_{ij} - \nabla \mathrm{p} + \rho \boldsymbol{F} \tag{2.20}$$

where ρ is the density of the fluid, **V** is the fluid velocity vector, τ_{ij} is the viscous stress tensor, p is the pressure and **F** is the body forces.

The energy equation is based on the principle that energy can neither be created nor destroyed but it can be conserved. It is also known as the first law of thermodynamics. The energy equation can be written as:

$$\rho \frac{De}{Dt} + \mathrm{p}(\nabla.\mathbf{V}) = \frac{\partial \mathrm{Q}}{\partial \mathrm{t}} - \nabla.\mathbf{q} + \boldsymbol{\Phi} \tag{2.21}$$

where e is the internal energy, t is the time, Q is the heat source, $\nabla.\mathbf{q}$ is the heat loss by conduction and $\boldsymbol{\Phi}$ is the dissipation term. The General conservation equations for momentum, energy and momentum are solved using the set of control volumes(Material, 2010).

$$\frac{\partial}{\partial t}\int_V \rho\emptyset dV + \oint_A \rho\emptyset \boldsymbol{V}.d\boldsymbol{A} = \oint_{\boldsymbol{A}} \Gamma_\phi \nabla\emptyset.d\boldsymbol{A} + \int_{\boldsymbol{V}} S_\emptyset dV \qquad (2.22)$$

The first, second, third and fourth terms represent the unsteady, convection, diffusion and generation term respectively. A process called discretization takes place which converts an algebraic equation into differential equations. CFD software usually works with differential equations to solve the fluid flow problems. The mesh handles geometric features of concern such as velocity, pressure and temperature gradients. To solve these equations in CFD, various discretization methods are used which include the Finite Difference Method (FDM), Finite Volume Method (FVM) and Finite Element Method (FEM). These equations can be suitable for inviscid flow, incompressible or compressible and steady or unsteady flow. In an inviscid flow, the viscous term is neglected and will be known as the Euler equation (Fabiano & Qiu, 2015), (Jamshed, 2015), (Caughey, 2004).

2.4.1 FINITE DIFFERENCE METHOD (FDM)

Finite Difference Method (FDM) is simply a method of derivative. It uses Taylor expansion series to develop derivatives of variables as the differences between values of the variable at several points in time or space. In a given function of x component of velocity *u*, the slope with respect to x can be determined as

$$\left(\frac{\partial u}{\partial x}\right)_i = \frac{u_{i+1}-u_i}{\Delta x} + O(\Delta x) \qquad (2.23)$$

where i and $i+1$ are the points for calculating the u values, Δx is grid spacing and $O(\Delta x)$ represent first order terms. Due to the error found in $\left(\frac{\partial u}{\partial x}\right)_i$ is called the truncation error. The truncation error is usually higher than $O(\Delta x)$ hence it is represented as first order. For second order and higher order, the equation becomes:

$$\frac{u_{i+1}-u_i}{\Delta x} + u_i = 0 \qquad (2.24)$$

2.4.2 FINITE VOLUME METHOD (FVM)

This the method used for most commercial CFD codes because it is better suited for modelling flow past complex geometries. FLUENT code uses the finite volume method while ANSYS uses finite element method. Finite volume uses shapes such as quadrilaterals rather than nodes. The quadrilaterals are usually referred as cells and a grid point as nodes. 2D cells are usually triangular cells while 3D cells are usually hexahedral, tetrahedral and prisms. Finite volume uses integral form of the conservation equations which are applied to a control volume and defined by a cell to get a discrete equation for each cell. Finite volume method sums up all the net mass flow into the control volume and set it to zero. By setting the mass flow to zero, the mass is conserved in the cell (Fabiano & Qiu, 2015).

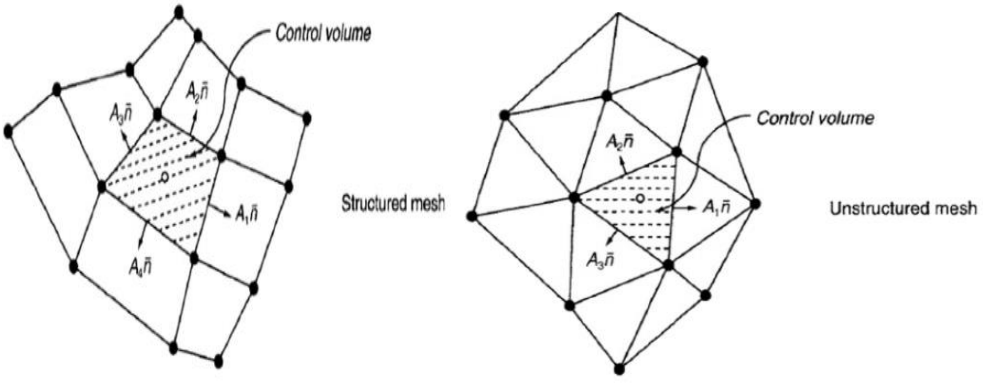

Figure 2-7: Structured And Unstructured Mesh For Finite Volume Method (Jamshed, 2015)

2.4.3 TURBULENCE MODELS

Fluid flows can either be laminar and turbulent. These flows are dependent on the Reynolds number. Reynolds number of a flow gives a measure of importance of inertia and viscous forces. A laminar flow is typically characterized by smooth varying velocity fields in space and time. In a laminar flow, the Reynolds number is usually below the critical Reynolds number. In a turbulent flow, the Reynolds number is above the critical Reynolds number ($Re_x \approx 100{,}000$) and a series of complicated events occur leading to a radical change in flow. In this state, the flow becomes random and chaotic. Turbulence models are a set of equations which can be algebraic or differential that determine the turbulent transport terms in a mean flow equation and hence close the systems of equation. These turbulence models include Sparlat Almaras (one equation) model, k-epsilon (two equations) model, k-omega (two equations) model and SST (four equations) model. Computational approaches to solving the turbulent fluid flows include: Direct Numerical Simulation (DNS), Large Eddy Simulation (LES) and Reynolds Averaged Navier Stokes (RANS) equations (Argyropoulos & Markatos, 2015).

Direct Numerical simulations resolves the wholes spectrum of scales in space and time. DNS involves numerically solving unsteady Navier Stokes equations. This type of simulation is not practical for industrial flow. Large Eddy Simulation solves filtered Navier Stokes equations (Poradowski, n.d.). The RANS model solves time averaged Navier stokes equations. RANS require the least computational power compared to LES, and DNS. The main objective of Reynolds time averaging is to translate any variable $\varphi\ (x, t)$, which is generally a function of space and time, and the sum of a mean and fluctuating component is expressed as:

$$\varphi\ (x, t) = \ \Phi(x) + \ \varphi'(x, t) \qquad (2.25)$$

Reynolds stresses is expressed as a tensor and it's a derivative of the Reynolds averaged momentum equation. Reynold's equations give an insight to the behavior of the turbulent stresses, but an engineer needs to find a method to close the equations before it can be used. The closure equations are the basis of turbulence modelling. The Boussinesq's eddy viscosity concept is used for modelling Reynolds stresses. It uses the analogy that the turbulent stresses are proportional to the mean velocity gradient. Models ranging from some simple algebraic models to complex models such as k-ε models can be used to simulate Reynolds stresses (Celik, 1999). The eddy viscosity is based on the number of transport equations:

1) Zero model equations:
    - Constant eddy-viscosity models
    - Mixing length models: l_0 specified geometrically; u_0 from mean flow gradients
2) One equation model:
    - l_0 specified geometrically; transport equation to derive u_o
3) two equation model:
    - transport equations for quantities from which u_0 and l_0 can be derived.

The most popular and beneficial CFD codes are the two equations models which are k-ε and k-ω models (Lieu, 2015)

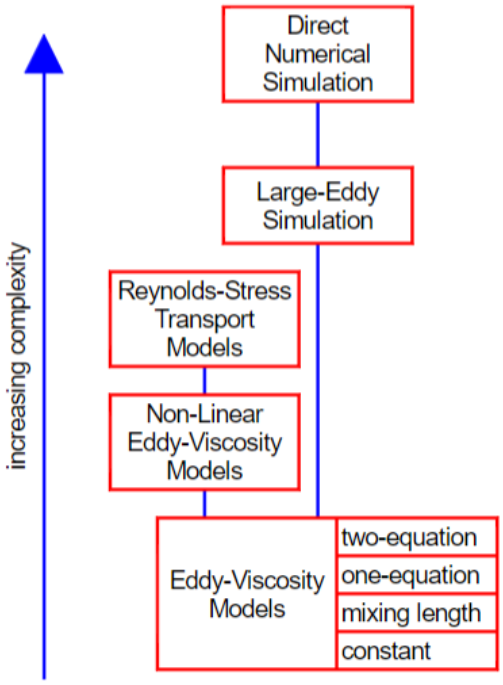

Figure 2-8: Turbulence Models And Their Order Of Complexities (Lieu, 2015)

3.0 DESIGN METHODOLOGY

This section describes the design process of the propellant tank in its "*pre*" and "*post*" manufacturing. The research study is carried out in three stages: the design of the propellant tank, numerical experiment on a C-D nozzle and testing stage of the propulsion system. A conceptual framework is developed to demonstrate the scope of the research. The figure below illustrates the process thought of the research study.

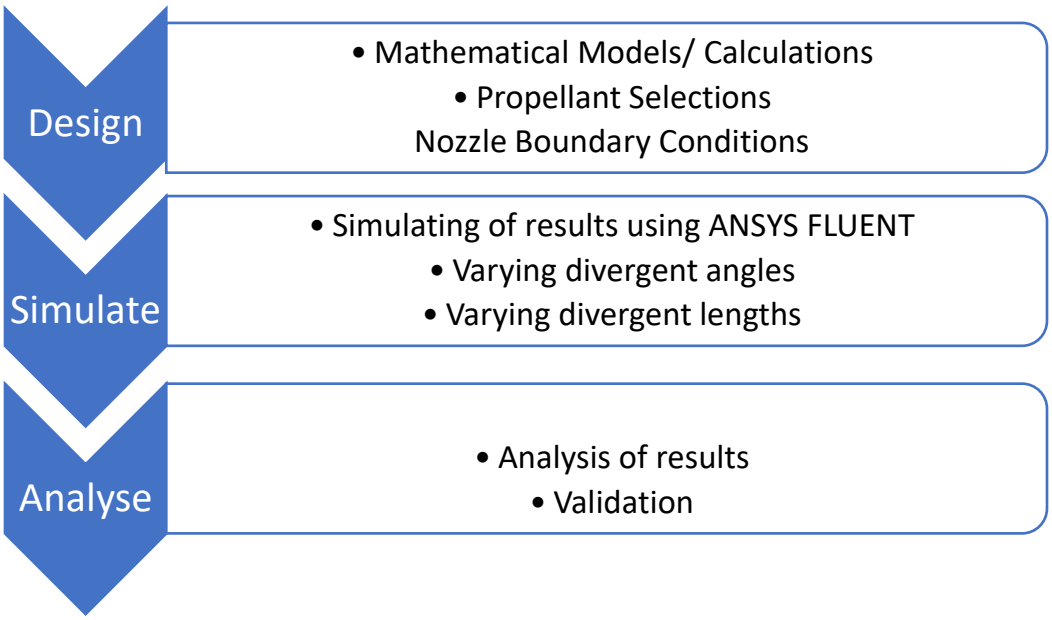

Figure 3-1: Conceptual Framework for Propulsion System

3.1 PROPELLANT SELECTION

Cold gas propulsion system's selection is based on the relatively low complexity, efficiency, thrust capabilities and low cost/power consumption. Many gases and liquids that are used as microsatellite's propellants are considered in this research study, which includes Oxygen (O_2), Nitrogen (N_2), Hydrogen (H_2), Carbon dioxide (CO_2), Helium (He), Xenon (Xe), Methane (CH_4), Propane (C_3H_8), Butane (C_4H_{10}), Air, 1,1,1,2- Tetrafluoroethne (R-134a) and 2,2-Dichloro-1,1,1-

trifluroethane (R-123). Newton third's law states that the high molecular weight is preferable for higher thrust. Recently, environmental issues had to be taken into considerations when designing therefore environmentally – friendly propellants are preferred. The use of a non-contaminating propellant is suitable as the expelled propellants would not have any residue, which may affect the mechanical actuators or sensing devices. Another factor to consider is the handling and storage of the propellants, hence a low boiling point and melting temperature are considered (Aysu, 2019).

Table 3-1: Properties Of Cold Gas Propellants (Sutton & Biblarz, 2010)

Propellant	Molecular Mass	Density (kg/m^3)	Specific heat	Theoretical Impulse (sec)
Hydrogen	2.0	28.35	1.40	284
Helium	4.0	56.70	1.67	179
Methane	16.0	225.86	1.30	114
Nitrogen	28.0	280	1.40	80
Air	28.9	402.06	1.40	74
Argon	39.9	200	35.3	57

Xenon is a heavy and inert gas. The viscosity of xenon increases with temperature withing a certain range this means the specific impulse is low when heating the gas. Methane, Propane and Butane are hydrocarbon which can be flammable and hence considered as hazardous gases. R-123 is classified as a Class II substance by Environmental Protection Agency (EPA) Clean Air Act (CAA) whose production and sales needs necessary certification and will be illegal after 2015 (Seubert et al., 2007). Carbon dioxide can be a suitable propellant, but it can be toxic if there are

any leakages. Table 3-2 shows a matrix analysis of cold gas propellants. This was done to justify the choice of the propellant. Previous studies indicates that Nitrogen, Helium, Hydrogen, Air and R-134a are the most suitable propellants for nanosatellites. These cold gas propellants are rated based on their safety, affordability, accessibility and performance. In the matrix analysis, 5 represent the high whereas 1 represent low.

Table 3-2: Matrix Analysis Of Cold Gas Propellants

Criteria	*N_2*	*He*	*H_2*	*Air*	*R-134a*
Safety	4	4	5	5	3
Affordability	5	3	4	5	4
Accessibility	4	3	5	5	4
Performance	5	2	2	4	4
Total	18	12	16	19	15

The table shows a comparative analysis of the cold gas propellant. It can be seen that Air is the most suitable propellant followed by Nitrogen. Looking at previous research conducted on cold gas thrusters, Nitrogen is usually the best option for its lack of reactivity, relatively low molecular mass and relatively high density. Nitrogen has propelling and thrusting heritage. The research study extensively looks at a comparative analysis between nitrogen and compressed air as propellants for microsatellite propulsion system's application.

3.2 MISSION DESIGN REQUIREMENTS

The design of the propulsion system is dependent on the size of the satellite. The propulsion system of the satellite is employed for station keeping, attitude control and de-orbiting among others.

Table 3-3: Mission Design Requirements

Satellite Type	Nanosatellite
Satellite Size	10kg
Orbit Type	Low Earth Orbit (LEO)
Operating Altitude	600-800 km
Ambient Pressure	1.013 bar
Ambient Temperature	298.15K
Mass of Propellant	0.00276 kg/s

3.3 CONCEPT OF OPERATION

The propellant tank is placed in the middle of the spacecraft to balance out the masses. In a cold gas propulsion system, the nozzle helps in the acceleration of exhausted gases from the tank, absorbing the fluid dynamic properties to produce thrust. The designed tank volume is 2.5litres, a suitable size for small spacecraft integration withstanding a maximum pressure of 60 MPA with a temperature threshold of 100 °C. The propellant is fed from the pressurized cold gas chamber to the thruster. The fill/vent valves are used as protection devices that help the rest of the system from being overflooded by high pressure. The pressure regulator helps in reducing the high pressure to the operational pressure in the nozzle. The solenoid valve aids in supplying the propellant to the thrust chamber.

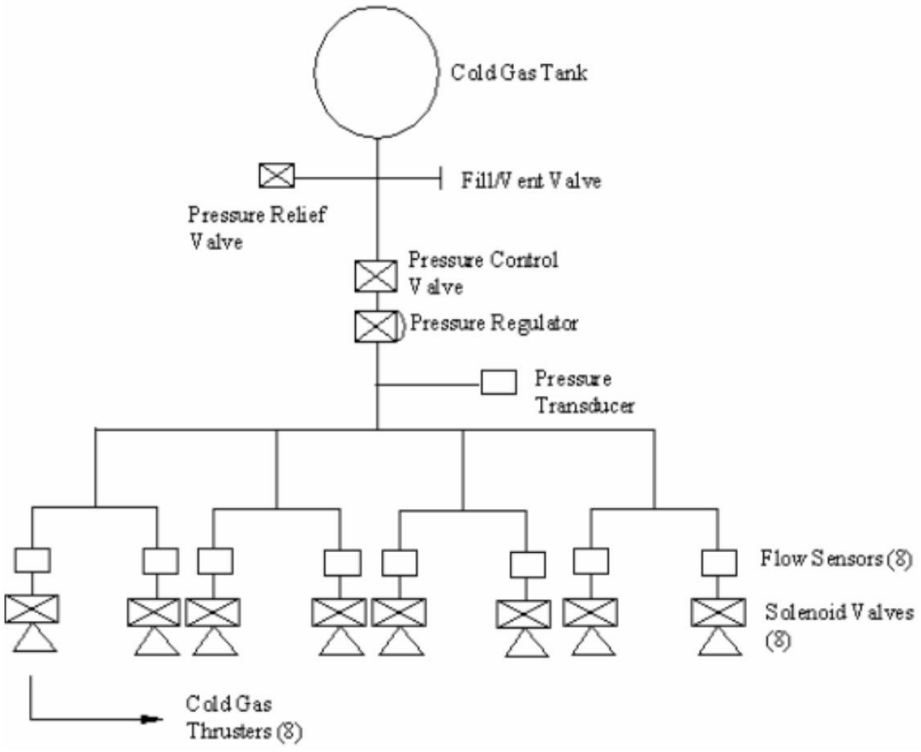

Figure 3-2: Flow Schematics Of A Propulsion System (Anis, 2012)

3.4 FLUID FLOW ANALYSIS

The CFD software used for this numerical experiment is ANSYS Fluent. ANSYS is divided into five (5) parts: structure, meshing, boundary setup, solution and results. A CFD Process Flow Chart is shown in Figure 3-3

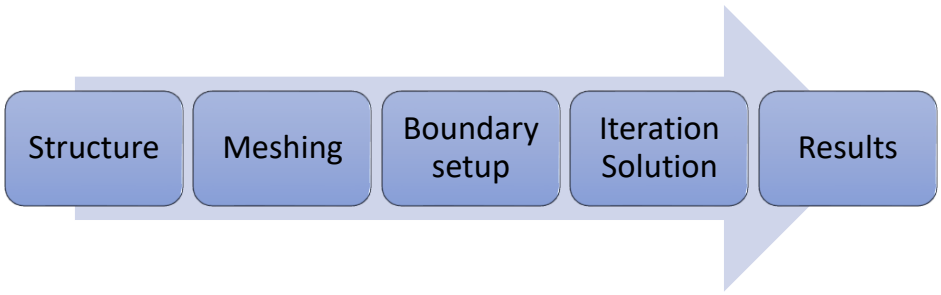

Figure 3-3: CFD Process Diagram

The nozzle is built virtually using SolidWorks software with adjusted parameters from the analytical calculations. The nozzle design is produced with six divergence angles; 5°,10°, 15°, 20°, 25° and 30° as shown in Figures 3-4 to 3-9. Table 3-4 presents the different divergence angle with its throat radius and expansion ratio derived from the CAD drawing in SolidWorks. The throat radius and inlet radius remain constant for divergence angles of 5°, 10°,15°, 20°, 25° and 30°. A two-dimensional geometry is used in the simulation to expedite the running time for each nozzle with varying divergence angle and divergence length.

Table 3-4: Divergence Angle with Nozzle Exit Radius and Expansion Ratio

Divergence angle	Exit Radius (mm)	Expansion Ratio
5	0.215	4.83
10	0.335	11.77
15	0.465	22.67
20	0.580	35.23
25	0.715	53.56
30	0.855	76.58

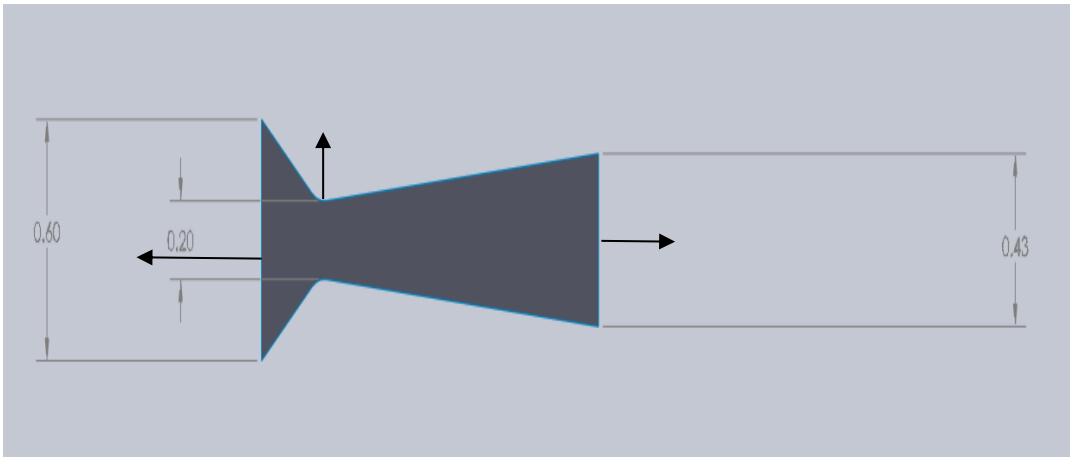

Figure 3-4: 5° Divergent Angle

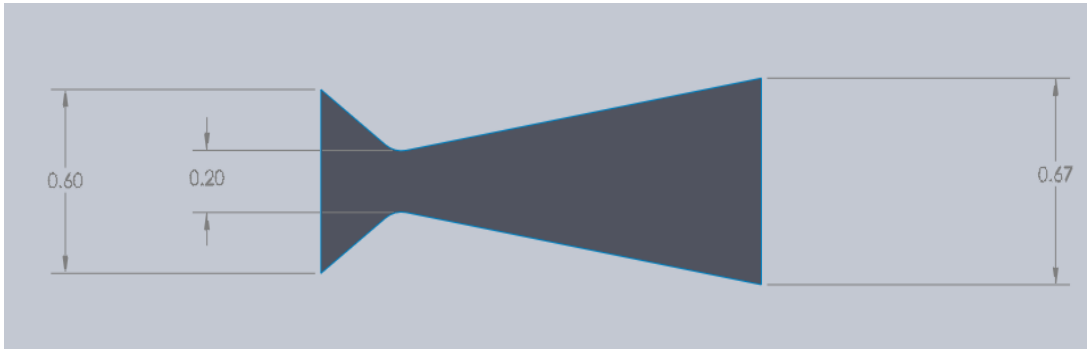

Figure 3-5: 10° Divergent Angle

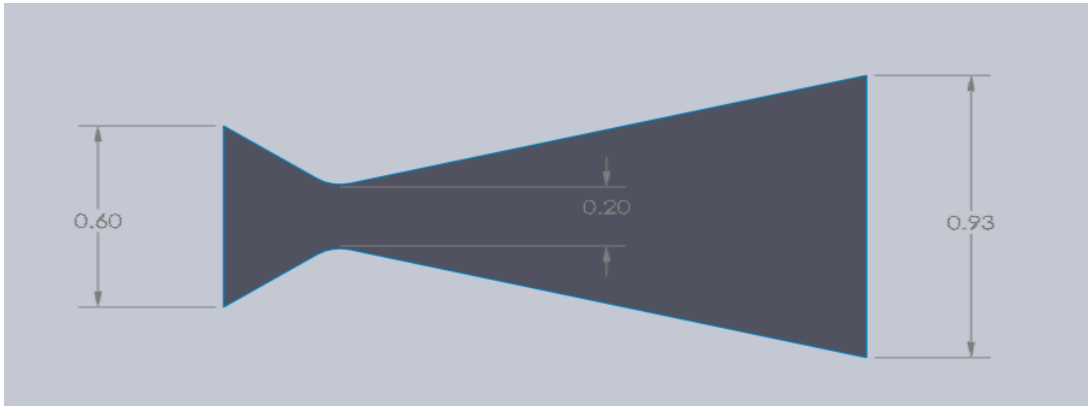

Figure 3-6: 15° Divergent Angle

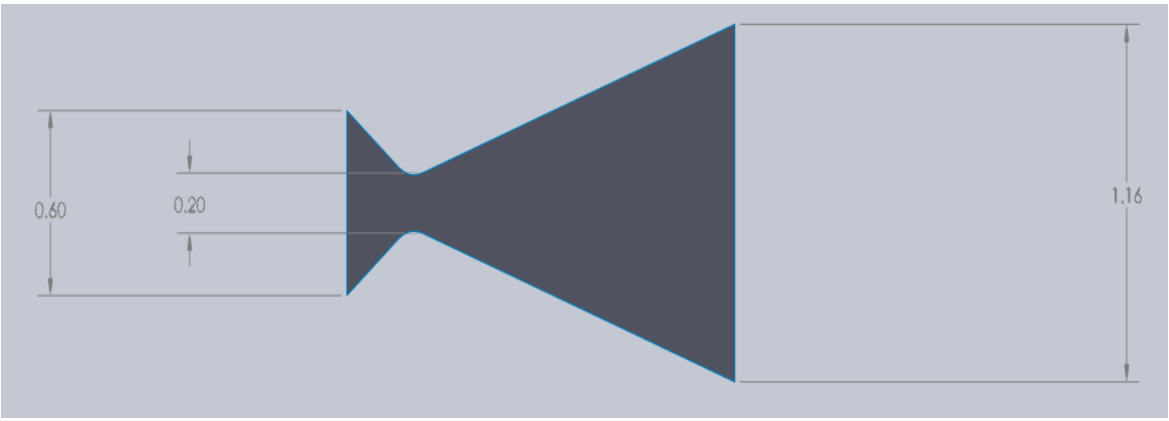

Figure 3-7: 20° Divergent Angle

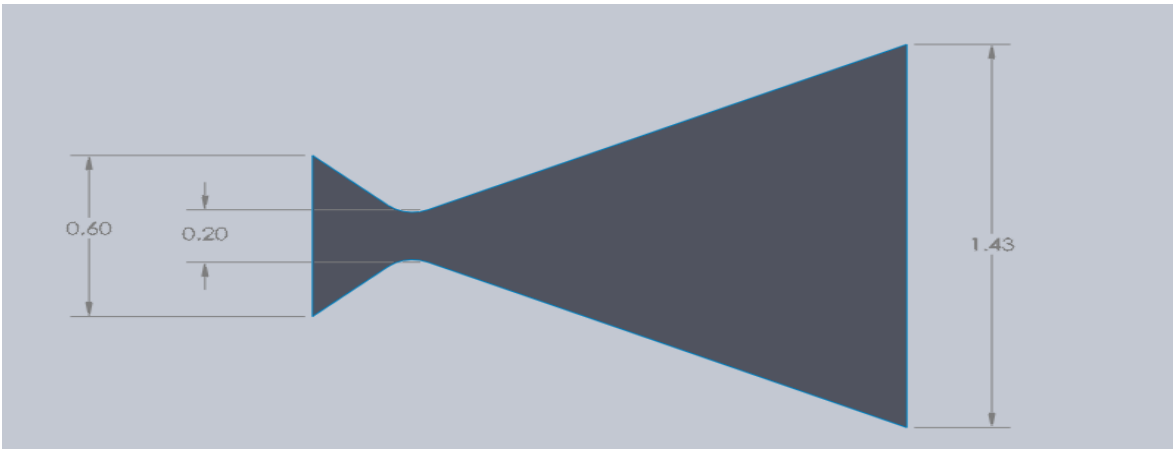

Figure 3-8: 25° Divergent Angle

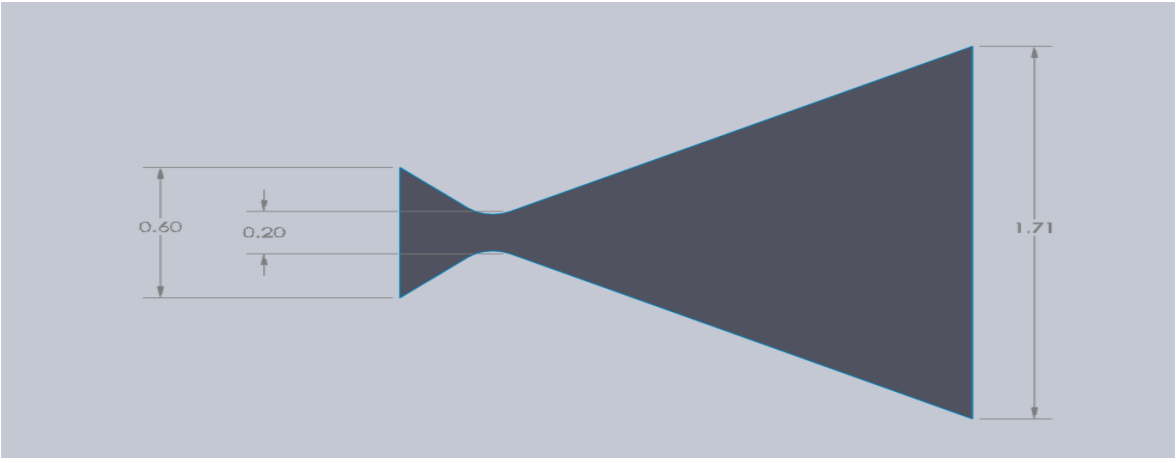

Figure 3-9: 30° Divergent Angle

The nozzles with different geometries are then imported into ANSYS Fluent CFD software for pre- and post-analyses. The in-built meshing tool in ANSYS Fluent enables the structure to be divided into finite set of control volumes for finite volume method of discretization. For the meshing sector, the nozzle structure follows a uniform 2-D structure, hence quadrilateral elements are used in the meshing with an element size of 0.001m.

The boundary setup is based on defining the material property; the numerical experiment uses air as the fluid material. The energy and standard k-ε turbulence models are activated to test the turbulence behavior within the nozzle (both near and way from the wall). The energy model activates heat transfer in the nozzle. The inlet pressure has a total gauge pressure and supersonic gauge pressure set at 2.432MPa with a total inlet temperature of 298K, which are calculated parameters from the analytical calculations. The outlet pressure has a gauge pressure of 101.325kPa and a backflow total temperature of 298K. The reference value is taken at the inlet for the calculations. A summary of the CFD inputs is presented in Table 3-5. To achieve convergence, the x-velocity, y-velocity, continuity and energy changes are required to be $1x10^{-6}$. In the iterative process, the discretized conservation equations are solved until it reaches convergence. Convergence is obtained when the changes in the solution variables are negligible, overall property conservation is achieved and quantities of interest have reached a stable value. The accuracy of the converged solution depends on the quality of the mesh, errors from numerical calculations, assumptions and physical models. Convergence occurred after 206 iterations. This is similar for all the six nozzle designs but with different numerical results. The graph below shows the convergence curve of the solution. The results are a final visual representation of the CFD process; a more detailed analysis is presented in the next chapter.

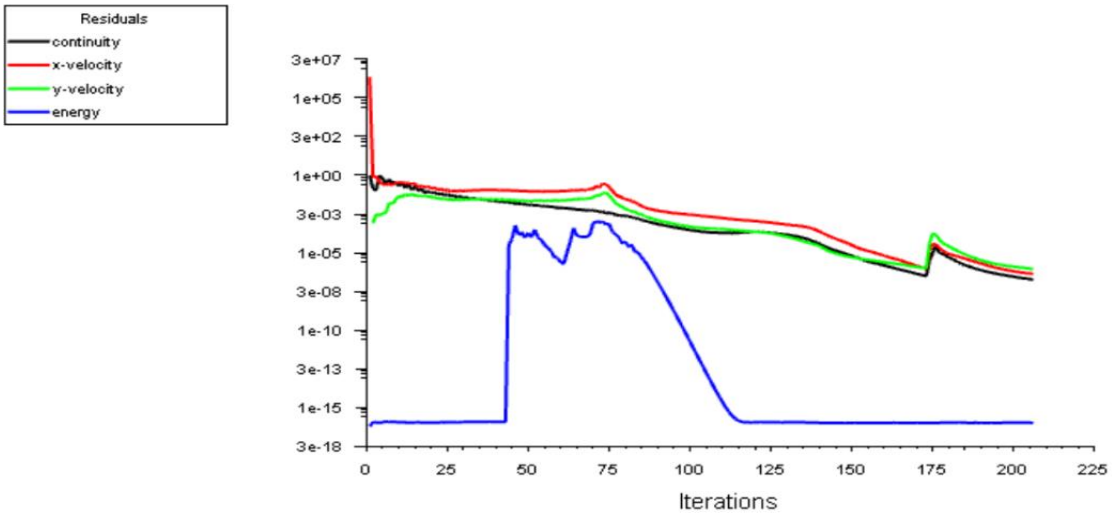

Figure 3-10: Convergence Plot

Table 3-5: CFD Inputs

Procedure	**Details**
Problem Setup General Solver	Type: Pressure Based Velocity: Absolute Time: Steady 2D space: Planar
Models	Energy: On Viscous: standard k-ε
Material	Fluid: Air Density: Ideal Gas
Boundary Conditions	Inlet: Pressure Inlet Gauge Pressure (Pa): 2.432×10^6 Inlet temperature (K): 298 Outlet: pressure Outlet Gauge Pressure (Pa): 101325

4.0 RESULTS AND DISCUSSION

This chapter presents and analyzes the numerical results obtained from CFD simulations based on the assumptions, convergence criterion and calculations performed using the boundary conditions documented in chapter 3. A combination of theoretical calculations and CFD simulations were done. This section highlights the comparative analysis of thermodynamic parameters and how the nozzle geometric affects the flow parameters within the C-D nozzle.

4.1 THEORECTICAL ANALYSIS

Table 4-1: Nozzle Parameters at T=298K

	Air		Nitrogen	
	Throat	**Exit**	**Throat**	**Exit**
Initial $\dot{m}$	0.0028	0.0028	0.0026	0.0026
$\mathbf{M_e}$	1	1.37	1	1.459
$\mathbf{A_e/A_t}$	1	1.099	1	1.495
P (bar)	1.918	3.091	1.928	3.506
T (K)	248	216	248	209
Isp (s)	32.75	41.91	32.75	43.83
V_e ***(m/s)***	340.3	466.21	340.3	496.5
$F_{calculated\ (N)}$	0.93	1.99	0.87	1.98
Final $\dot{m}$ **(kg/ s)**	0.0029	0.0048	0.0027	0.0046

Based on the equations presented in chapter 2, Table 4.1 is created. The designed thrust for the C-D nozzle is 2N. Hence, all assumptions and calculations are based on the designed thrust level.

The analytical modelling uses Microsoft Excel software to compute the values below. The nozzle parameters (throat and exit) for Air as a propellant are compared to Nitrogen. Air has a molecular mass of 28.96 g/mol in contrast to Nitrogen with a molecular mass 28 g/mol.

The analytical model in Table 4-1 illustrates slight changes in the nozzle parameters. The temperature, specific impulse (Isp) and velocity at the throat remain constant for both Nitrogen and Air. Exit Mach number for air is calculated to be 1.37 with an associated exit Isp of 41.91s and Nitrogen has an exit Mach number of 1.459 with an associated Isp of 43.83s at the exit. These observations can lead to the conclusion that Nitrogen has a higher Isp than air as presented in literature. The graph in Figure 4-1 also shows Nitrogen having a higher specific impulse than Air at the supersonic region. At the subsonic region, the Isp is the similar.

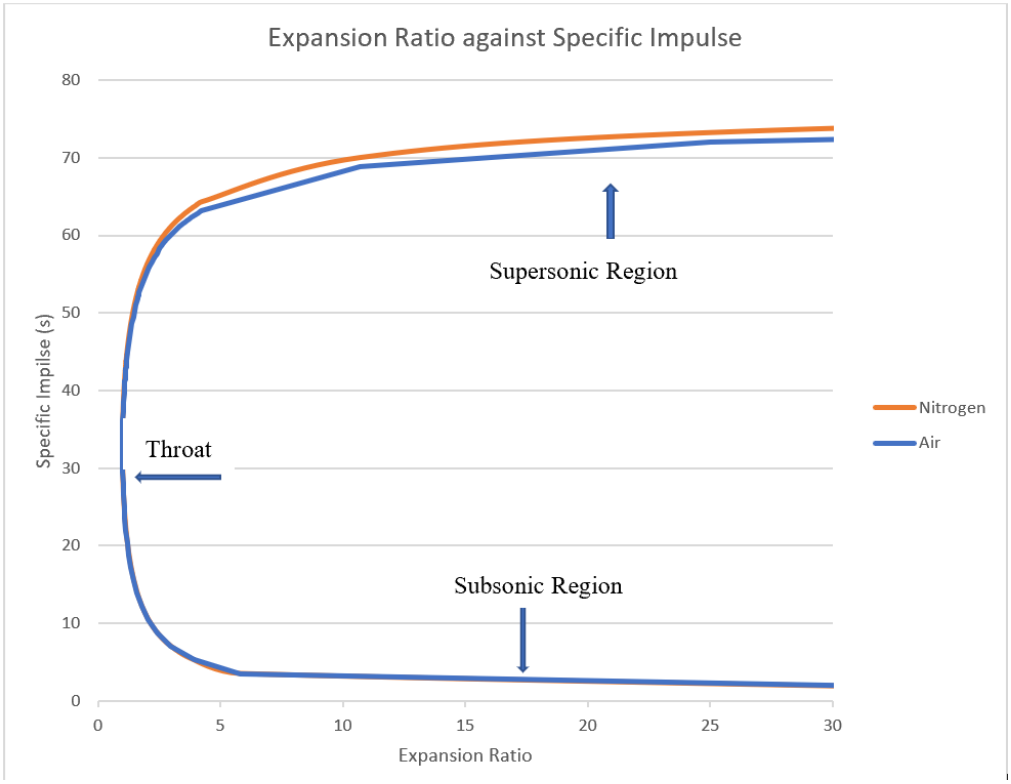

Figure 4-1: Graphical Representation Of An Expansion Ratio Against Specific Impulse For Nitrogen And Air

Analytical calculations have provided information on the nozzle parameters at the exit and throat. As compressed air is moving from the pressurized tank to the nozzle at a high temperature, a pressure analysis is conducted to attain the suitable inlet pressure. Figure 4-2 plots the throat diameter (Dt) and the nozzle exit diameter (De) against the regulator pressure. The pressure regulator (P_r) supplies gas to the nozzle at a specific pressure. The chamber pressure equals the regulator pressure. The following equations are used to generate the graph.

$$A_t = \frac{\dot{m}C^*}{P_r} \tag{4.1}$$

$$A_e = A_t \tag{4.2}$$

$$D_t = 2\sqrt{\frac{A_t}{\pi}} \tag{4.3}$$

where ε is the area expansion ratio

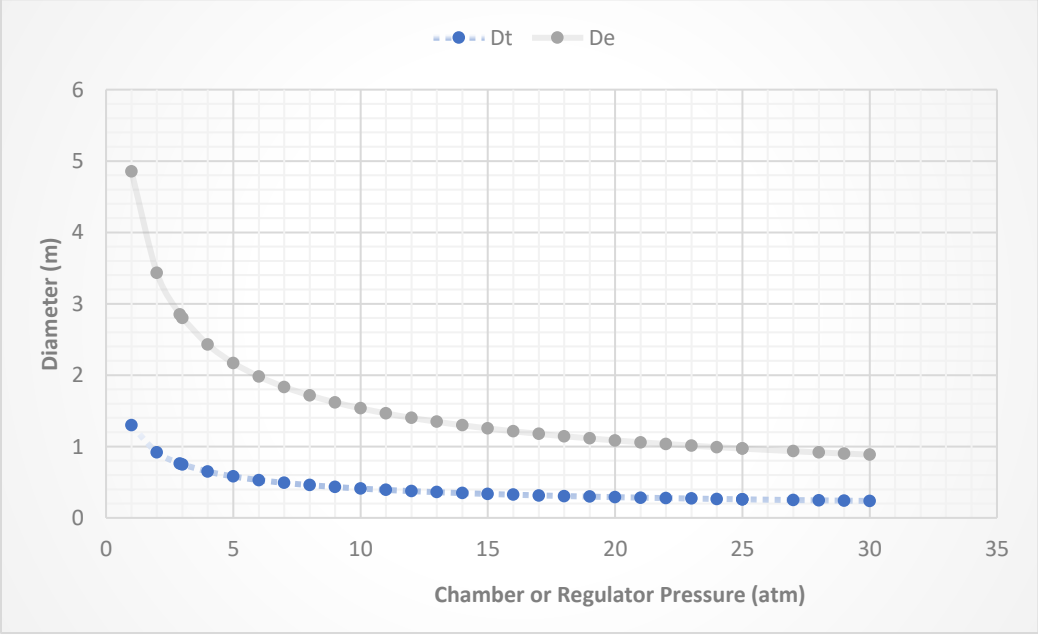

Figure 4-2:Nozzle Diameters vs. Regulator Pressure

The nozzles have a constant throat diameter of 0.09m. From the graph, at a throat diameter of 0.09m, an associated regulator pressure is 25atm (2.432 x10^6 Pa). This is used as the inlet pressure for the CFD simulation. The additional results obtained from the CFD simulation are analyzed later in this chapter. The properties at different divergence angles form the analytical calculations were further analyzed and can be seen in Table 4-2.

Table 4-2: Analytical Nozzle Parameters At Different Divergent Angles

Divergence Angle (degree)	Me	Ve (m/s)	Po/P	P (bar)	To/T	T (K)	Isp calculated (sec)	Delta V (m/s)
5	3.138	1067.86	0.022164	45	2.69	100.356	64.23	4.426
10	4.105	1396.93	0.005731	176.7962	4.37	68.18	69.26	4.77
15	4.85	1650.46	0.002255	449.24	5.70	52.24	71.63	4.93
20	5.44	1851.23	0.001148	882.69	6.92	43.07	72.949	5.03
25	6.01	2045.20	0.00627	1616.26	8.22	36.23	73.92	5.09
30	6.51	2215.35	0.000382	2654.04	9.48	36.23	73.92	5.09

The divergence angles are further examined to investigate the effects on the fluid flow parameters. Available nozzle literature proposes the use of a divergence angle of 15° as the ideal in a bid to avoid flow separation and consequential shock wave generation. This research study employs compressed air as a propellant for the CFD simulations at divergence angles of 5°,10°, 15°, 20°, 25°and 30° to study the influence of divergence angle variation on fluid flow parameters of interest.

4.2 NOZZLE DIVERGENT ANGLE

The variation of nozzle divergence angle is studied to establish an optimal divergence angle for a C-D nozzle suitable for microsatellite propulsion system using compressed air as a propellant. The profiles of flow parameters of interest, which include pressure, temperature, velocity and Mach number are plotted and analyzed. The contour plots for the aforementioned flow parameters at various convergence angles are presented in Appendix A.

4.2.1 PRESSURE PROFILE

The pressure profile shows a variation in pressure distribution from 5° to 30° divergence angles. The pressure starts from a regulator's inlet pressure of 2.432 MPa. The pressure regulator reduces the pressure from the chamber pressure to the operating pressure. The simulation is based on a pressure inlet/outlet boundary condition. Hence, all calculations are carried out on this basis. The exit pressure is initialized at atmospheric pressure (101.325kPa). Figure 4-3 and 4-4 shows a graphical representation of pressure distribution for each of the divergence angles obtained from the CFD simulation. Figure 4-3 illustrates a combination of all the divergent angles in one graph whereas Figure 4-4 shows them individually. From the graph, the throat is located at 0.32m.

The divergence angles of 5°,10° and 15° shows similar shape with little variations. At 5°, there are moments of normal shocks taking place downstream of the throat before the nozzle exit. The pressure finally reduced to 89.214 kPa at the outlet. The 10° divergent angles showed less shocks compared to the 5° divergence angle. It is observed to have an exit pressure of 84.292kPa. At 15° divergence angle, it is observed that after the choking condition at the throat, the pressure reduced to a final exit pressure of 60.551kPa.

The divergence angles for 20°,25° and 30° all had similar pressure profile with an exit pressure of 29.087 kPa, 22.245 kPa and 17.425 kPa respectively. It was scientifically observed that they all follow the exit shock condition as discussed in Chapter two. This may be concluded because the pressure is increasing outside the nozzle exit plane.

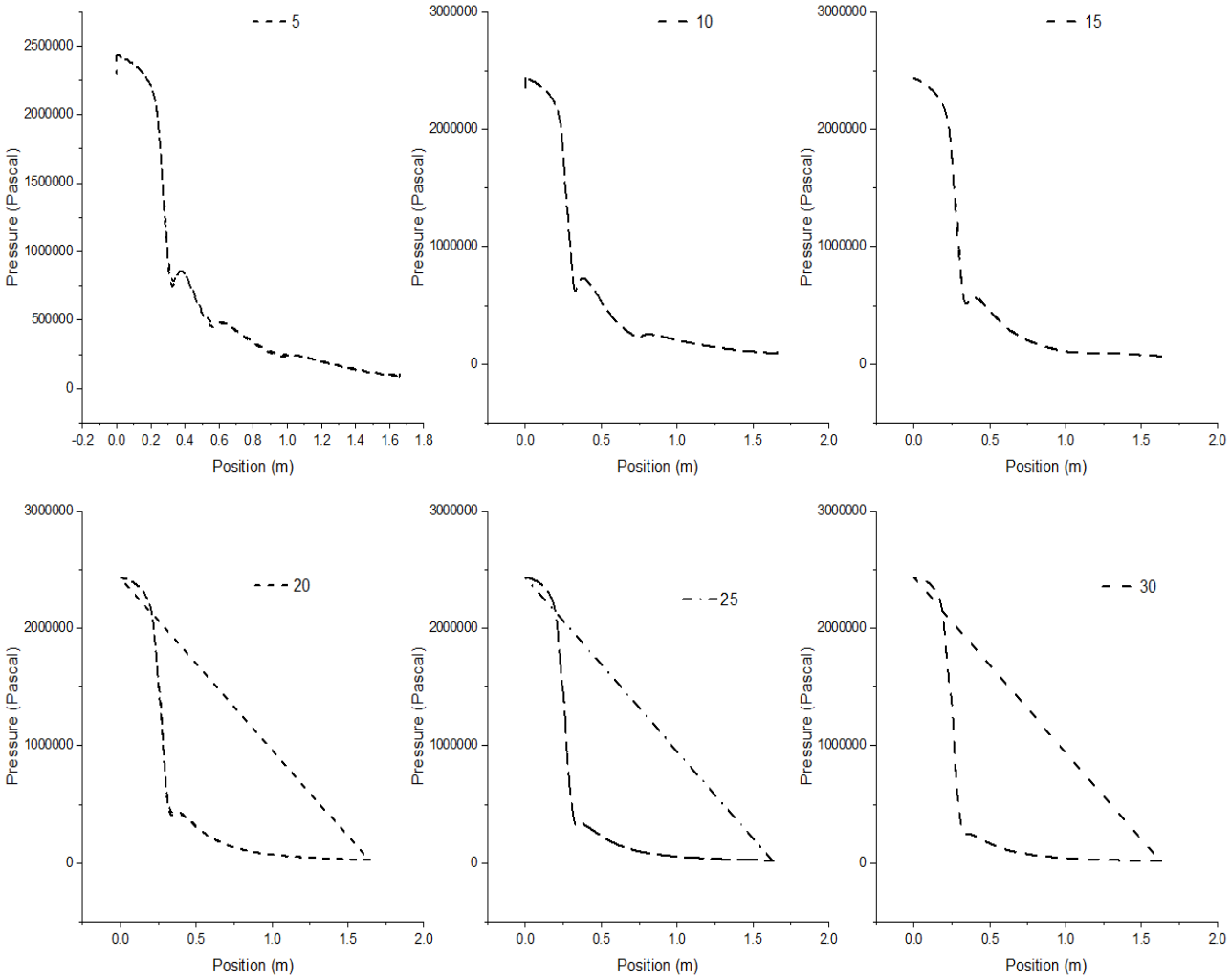

Figure 4-3: Single Pressure Profile

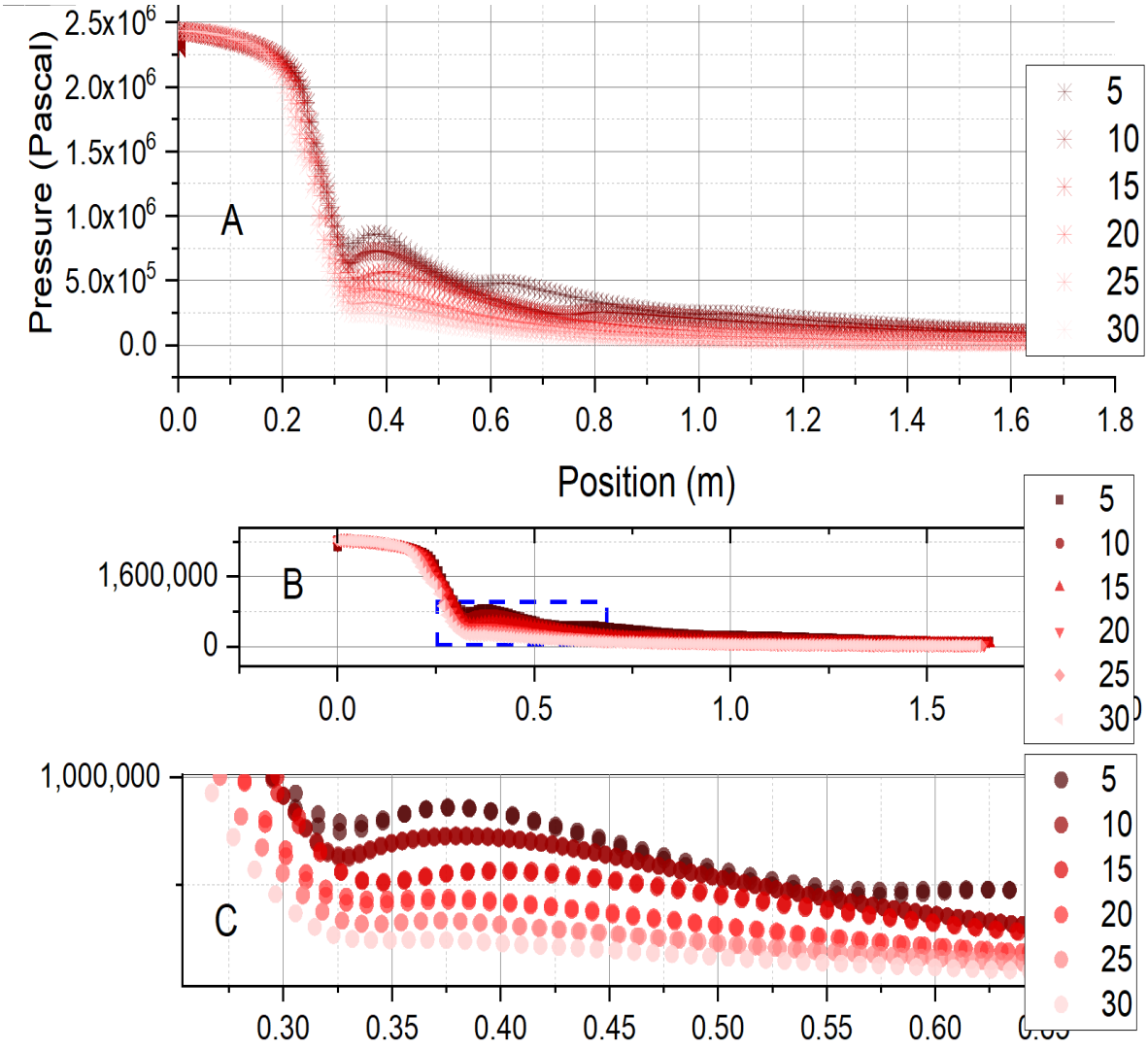

Figure 4-4: Combo Pressure Profiles with Focus on The Throat Region

The initial starting pressure drops slightly after the computation. The input value is 2.432 MPa but the inlet value after computation is shown as 2.430MPa for 5°, 2.431 MPa for 10°, 2.429 MPa for 15°, 2.431 MPa for 20°,25° and 30° respectively. This drop may be as a result of pressure loss taken place at the inlet section of the nozzle. The pressure profiles in Figure 4-4 reduce across the nozzle with the exception of 20°,25° and 30° divergence angles which have a limiting case of Navier Stokes equation due to its large surface area at the divergent section.

4.2.2 TEMPERATURE PROFILE

The temperature profile follows the same shape as the pressure profile discussed in section 4.2.1. As the pressure increases in a nozzle, the temperature also increases and vice versa. The temperature starts with an inlet temperature of 298K. Figure 4-5 and 4-6 show the graphical representation of temperature profiles of the divergent angles derived from the CFD simulation. Figure 4-5 illustrates a combination temperature plots of all the divergence angles in one graph whereas Figure 4-6 shows them individually.

The nozzle divergent angles of 5°,10°, 15° shows similar shape with little variations. At 5°, due to the chocking and shocking conditions, the final exit temperature is observed at 143.54K. The 10° divergence angle had less shocks compared to the 5° angle. It was observed to have an exit temperature of 116K. At 15°, it was observed that after the choking condition at the throat, the temperature reduces to a final exit temperature of 104K. The divergence angles for 20°,25° and 30° all had similar temperature profile with an exit temperature of 86K, 78K and 73K respectively.

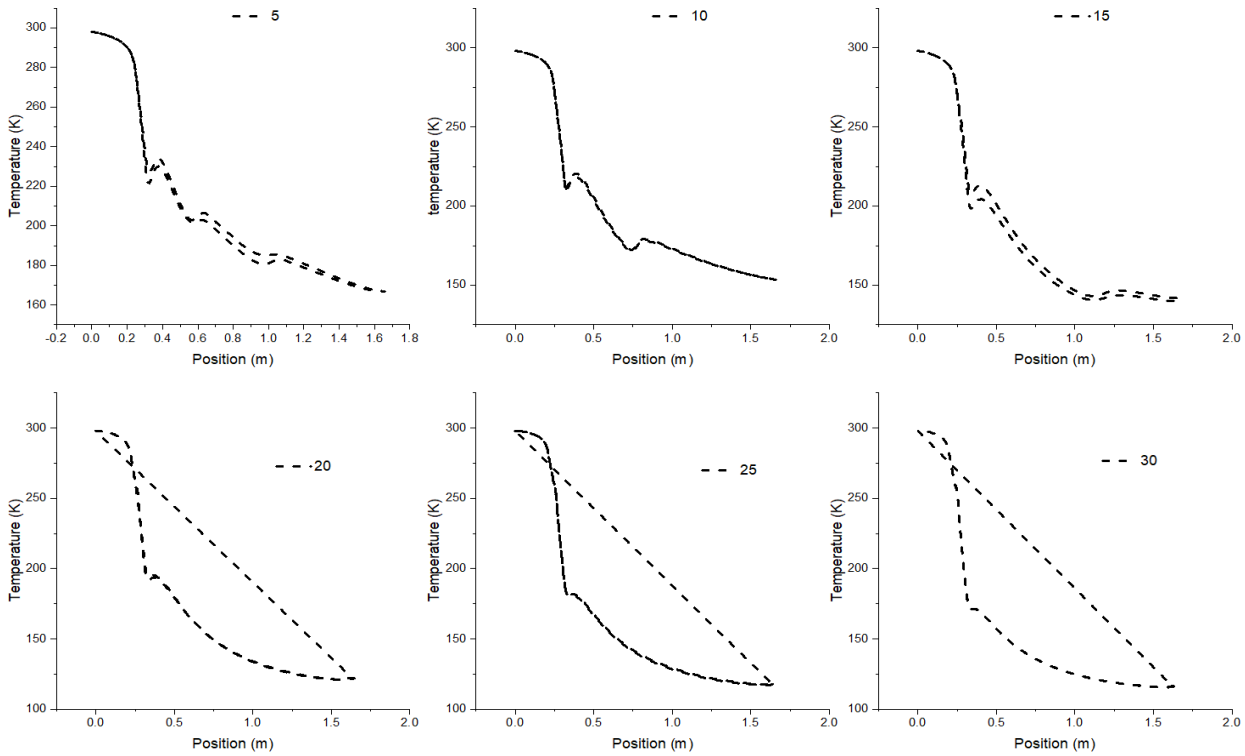

Figure 4-5: Single Temperature Profile

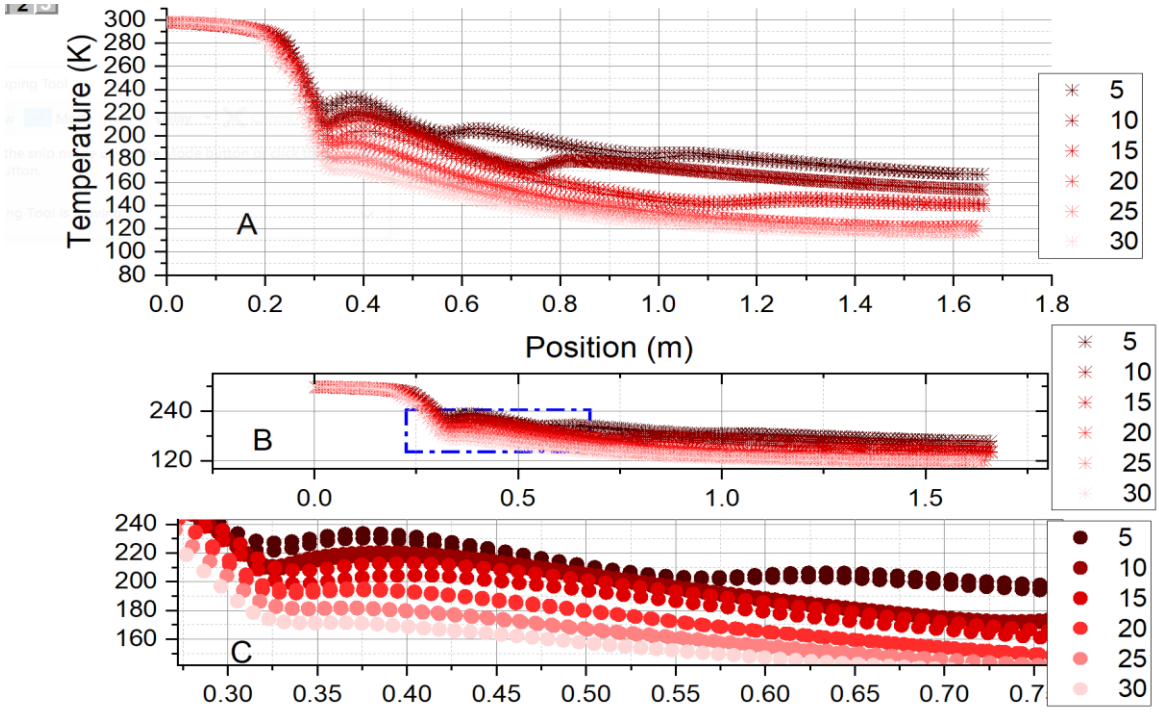

Figure 4-6: Combo Temperature Profiles with Focus on The Throat Region

The initial starting temperature drops slightly after the computation. The input value was 298K but the inlet value after computation is shown as 297K for all the divergence angles. This slight change can result from heat losses taken place at the inlet section of the nozzle. The temperature profiles in Figure 4-6 reduce across the nozzle with the exception for 20°,25° and 30° which have a limiting case of Navier Stokes equation due to its large surface area at the divergent section.

4.2.3 VELOCITY PROFILE

As the pressure and temperature reduce across the nozzle, the velocity increases in the nozzle. The turbulence model used is a standard k-ε turbulence model, therefore the species scattered throughout the nozzle and hence it is hard to compare with other divergent angles. To best interpret the velocity results, the Mach number is plotted as a function of velocity. Figure 4-7 and 4-8 show a graphical representation of Mach number for each of the divergent angles derived from the CFD simulation. Figure 4-7 illustrates a combination of all the divergence angles in one graph whereas Figure 4-8 depicts them individually.

The Mach number profile shows a variation in Mach number distribution from 5° to 30° divergence angles. The Mach number started at an estimated Mach number of 0 and increases to 2.32 for 5° divergence angle after the chocking condition and shocks occurring downstream of the nozzle. The 10° divergence angles has less shocks compared to the 5° angle. It is observed to have an exit Mach number of 2.8. At 15°, the observed Mach number after the choking effects was 3.05. The divergence angles for 20°,25° and 30° all have similar pressure profile with exit Mach numbers of 3.51,3.75 and 3.92 respectively.

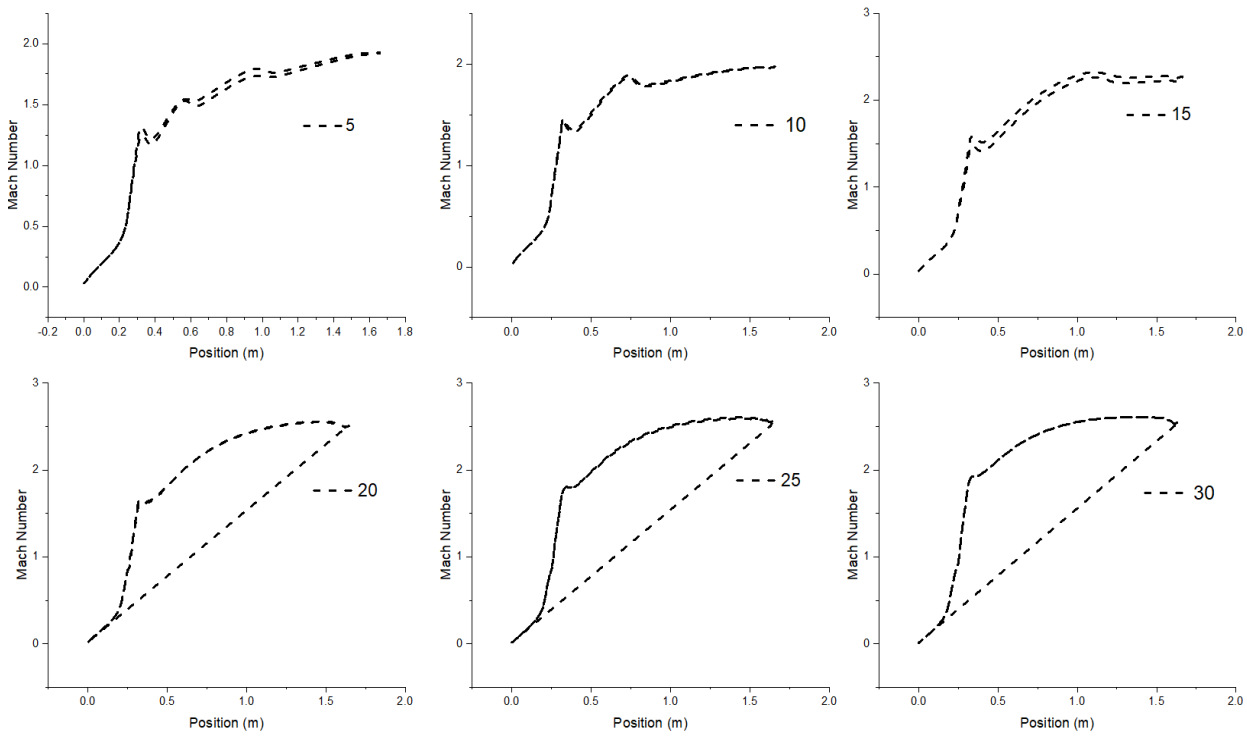

Figure 4-7: Single Mach Number Profiles

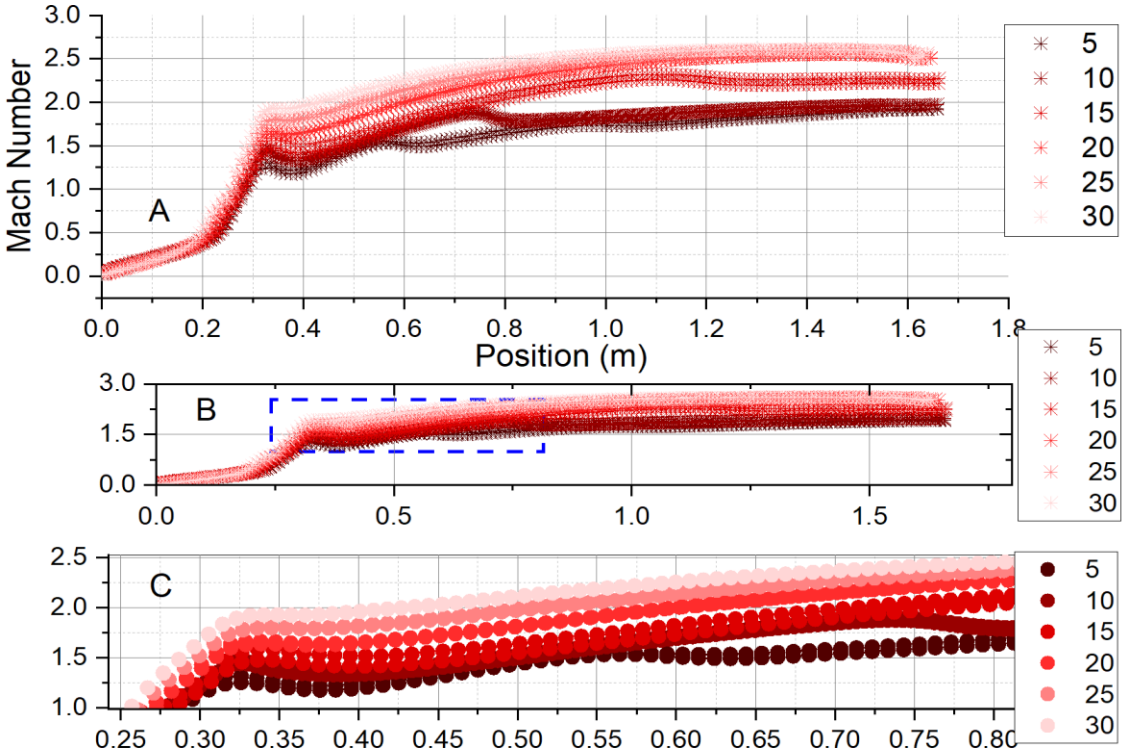

Figure 4-8: Combo Mach Number Profiles with Focus On The Throat Region

As the Mach number is a function of velocity, it can be observed that the velocity increases across the nozzle. The exit velocities from the CFD computation are 558m/s, 606m/s, 624.97m/s, 654m/s, 665m/s and 672m/s for 5°,10°,15°,25° and 30° respectively. Table 4-3 shows a summary of the temperature, pressure, velocity and exit Mach number.

Table 4-3: Summary of CFD Results

	Temperature (K)	**Pressure (Pa)**	**Velocity (m/s)**	**Exit Mach**
	Min.	Min.	Max	
5°	144	89214.48	558.18	2.32
10°	116	89292.09	606.29	2.8
15°	104	60551.53	624.97	3.05
20°	86	29087.20	654.08	3.51
25°	78	22245.25	665	3.75
30°	73	17425	672	3.92

4.3 NOZZLE DIVERGENT LENGTH

The influence of nozzle convergence length on nozzle design parameters is also investigated. The divergence angles section shows a difference in the back pressure in each of the divergence angles at the supersonic exit pressure of 101.325kPa. This research outcome leads to testing the effects of the divergence length of a C-D nozzle using compressed air as gaseous propellant. The divergent angles of 5°, 10°, 20°, 25°, 30° have either multiple shocks or limiting case of Navier-Stokes equations, hence there are not considered in this study. The divergence length of the previous divergence angles variation study is a constant value of 1.38m. This study focuses on varying the divergence length of the nozzle for 15°, 16° and 17° divergence angles. The divergence angles are adjusted to suit the simulation such as 1.20m and 1.25m. The divergence length of 1.20m has a divergence angle of 17° whereas the divergence length of 1.25m has a divergence angle of 16°. The lengths are studied based on their pressure, velocity and Mach number. The same boundary

conditions are used as in previous study on divergence angles variation. The geometry at various convergence length is presented in Appendix B.

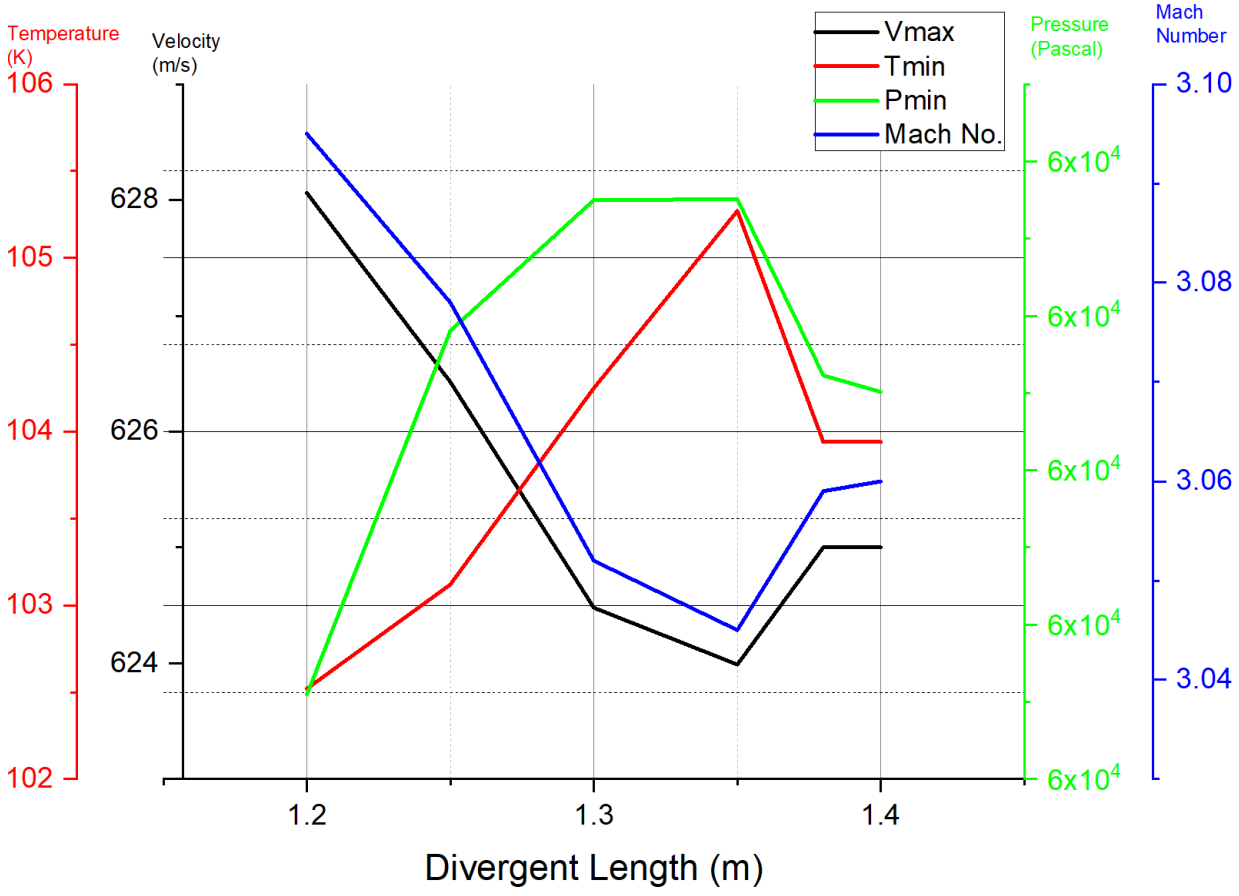

Figure 4-9: Divergence Length Parameters

Figure 4-9 shows a multi-Y graph with reference to the temperature, velocity, pressure and Mach number. V_{max} represent the maximum velocity at the end of the nozzle, T_{min} represents the minimum temperature at the exit, and P_{min} stands for the minimum pressure at the exit. The following observations can be deduced from the divergence length computations:

- Velocity decreases across the divergence length but reached a rise at 1.35m where it became stable

- Temperature increases till the divergence length of 1.35m where it starts to decrease and remain constant
- Pressure increases till 1.30mm where it maintains stability and starts to decrease and later remains constant at 1.40mm.
- The Mach number which is a derivative of velocity, follows the same trend as the velocity profile.

However, the divergence length of 1.35m has a generally high peak for the minimum temperature and minimum pressure and at the same time produces low velocity. The 15^0-divergence angle has a minimum pressure value of 61.756kPa, which is close to the exit pressure of 101.325kPa compared to the other divergence angles.

Reference	Mass of satellite (kg)	Expansion Ratio	Divergence Angle	Throat Radius (mm)	Thrust Produced
	1.33	10	15	0.97	
	1-20	15	28	0.06	2.24 mN
My work	10	22.	15	1	2N

5.0 CONCLUSION AND RECOMMENDATION

Present numerical study is based on theoretical calculations and computational simulations of a cold gas propulsion system. Physical situations typically vary from analytical calculations. Firstly, the nozzle geometry calculated from theory has to be adapted during simulation process as the values make sense mathematically but could not comply to structural analysis in SolidWorks.

It is further observed that by changing the divergence angle of a C-D nozzle, the divergence length and the expansion ratio change. The number of shocks reduces across the divergence angles but is eliminated at 15°. The divergence angles of 20°, 25°, 30° have a limited case of normal shocks as the shocks occurred outside of the nozzle. This is not a favorable criterion for nozzle design. The exit pressure for 15° divergence angle with a divergence length of 1.38m is 60.551kPa which is 40% difference compared to the ambient pressure of 101.325kPa.

The variation of divergence length evidently affects the flow parameters of a C-D nozzle. The divergence length of 1.35m with a divergence angle of 15° yields an exit pressure of 61.756kPa (39% difference). The marginal difference in exit pressure could be due to the type of turbulence model employed for the simulation. According to published literature, this seems to be a good nozzle design as its exit pressure is slightly below the ambient pressure.

5.1 RECOMMENDATION

The study can be divided into:

- Further numerical investigation on the convergence angle and convergence length variation while maintaining the same divergence parameters and boundary conditions
- Effects of the pressure ratio variation on a C-D nozzle design parameters.

- The research work can dive into prototype development and testing stage. The fabrication stage can make use of the novel additive manufacturing technology. This technology is currently a popular technique used in the manufacturing of satellites components.
- Exploring different materials of additive manufacturing technology and testing to compare CFD results with flights results.
- Comparison between different type of nozzles and their flow parameters.

APPENDIX A:

Pressure Contour at 5° Divergence Angle:

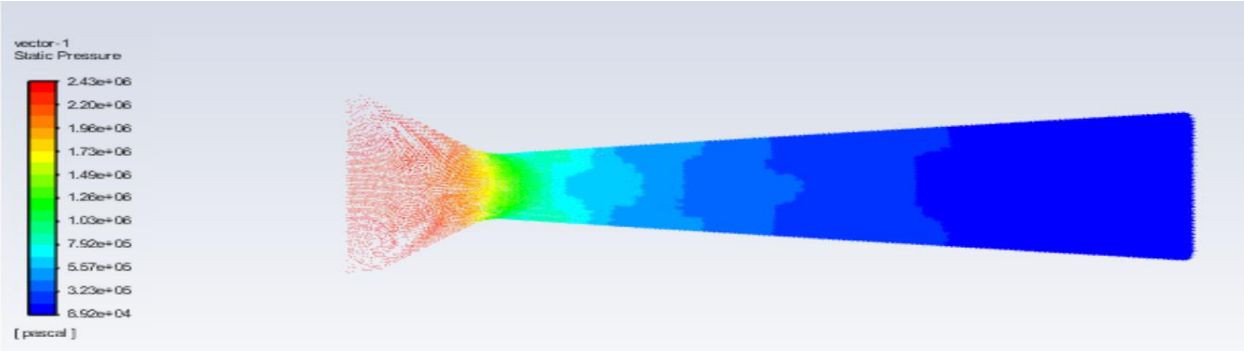

Velocity Contour at 5° Divergence Angle:

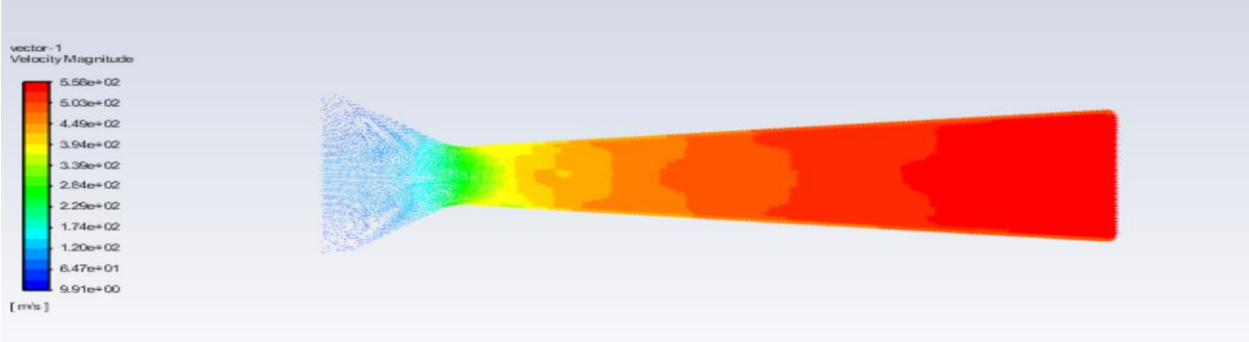

Temperature Contour at 5° Divergence Angle :

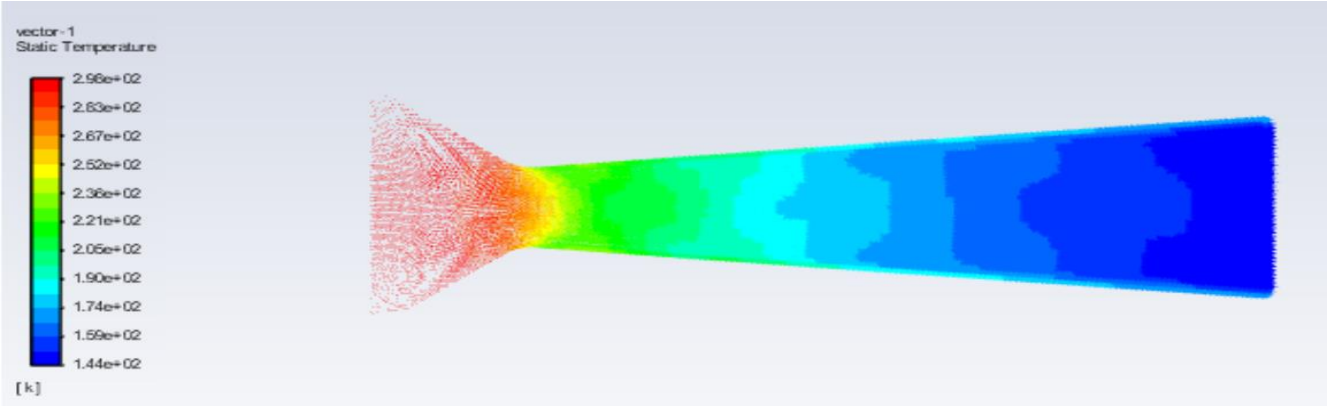

Pressure Contour at 10° Divergence Angle:

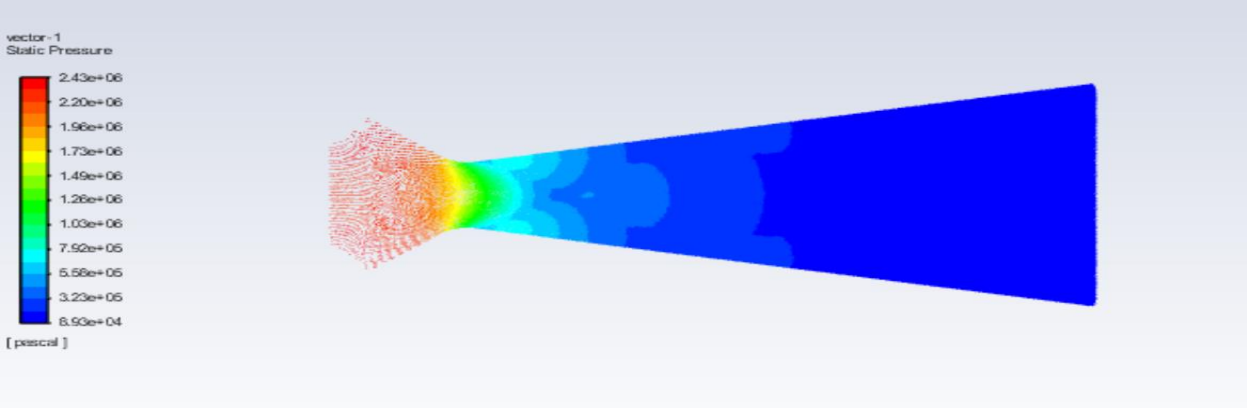

Velocity Contour at 10° Divergence Angle:

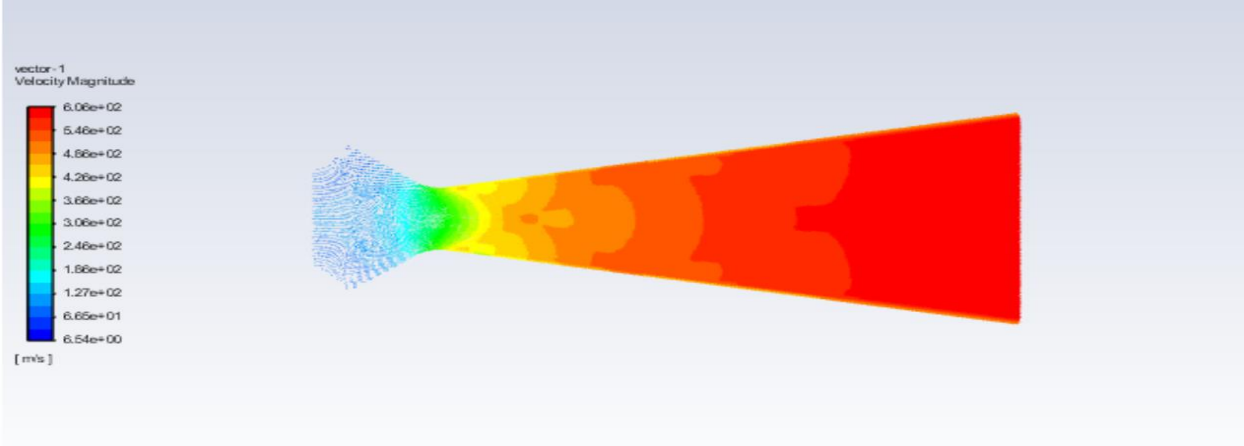

Temperature Contour at 10° Divergence Angle

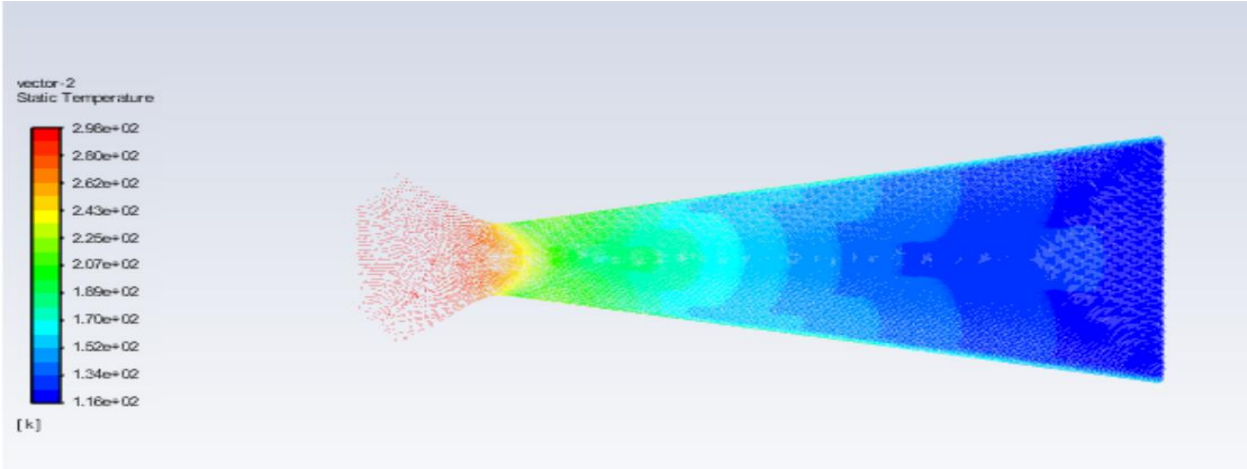

Pressure Contour at 15° Divergence Angle:

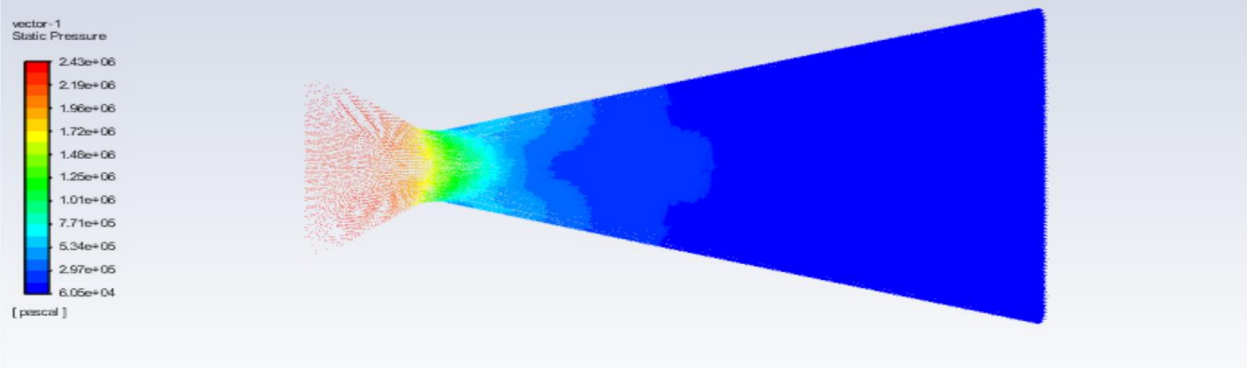

Velocity Contour at 15° Divergence Angle:

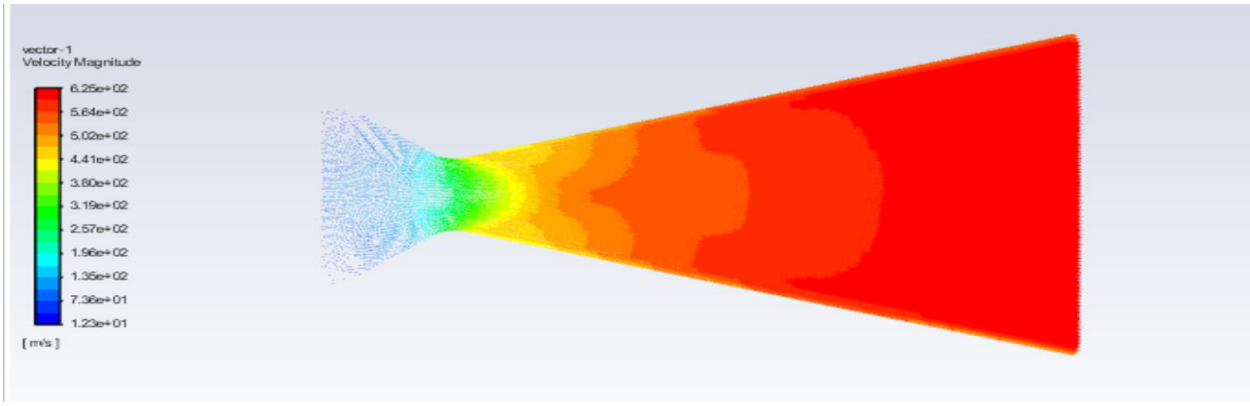

Temperature Contour at 15° Divergence Angle:

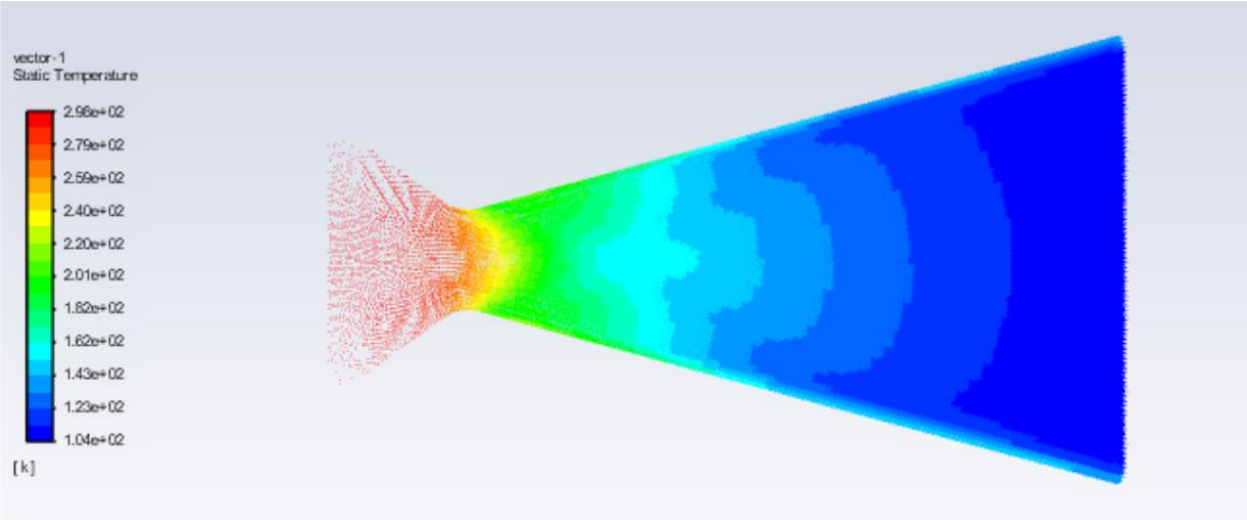

Pressure Contour at 20° Divergence Angle:

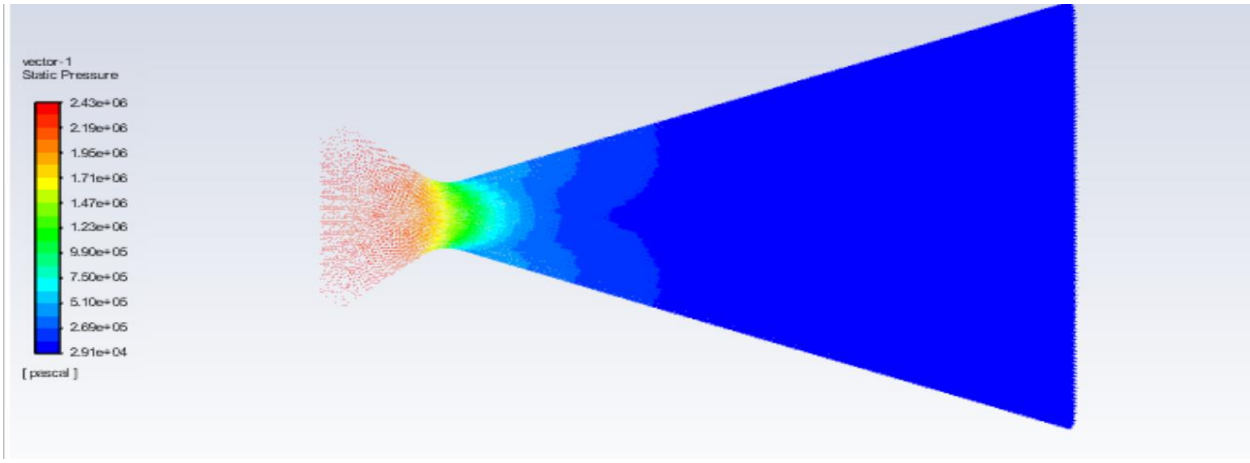

Velocity Contour at 20° Divergence Angle:

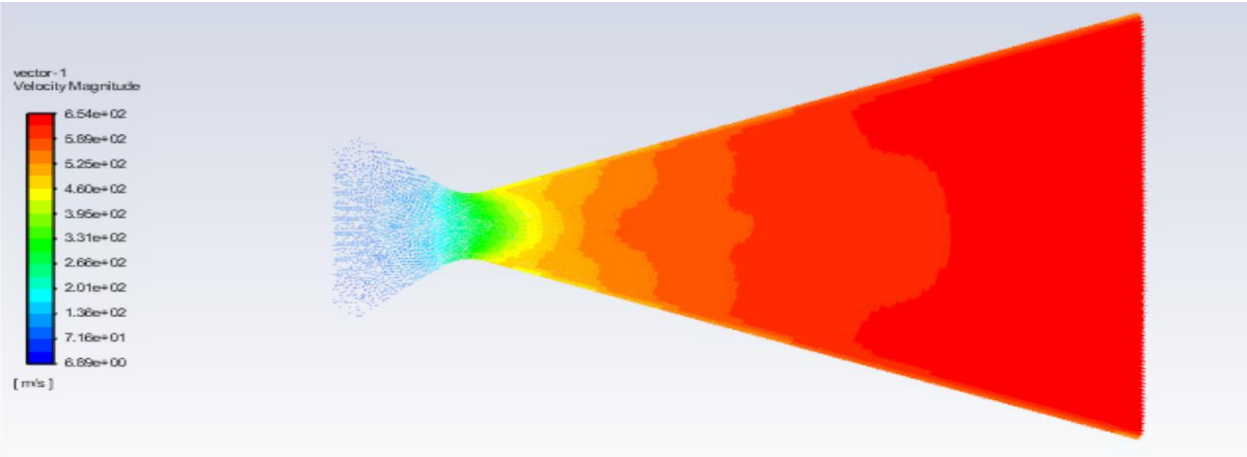

Temperature Contour at 20° Divergence Angle:

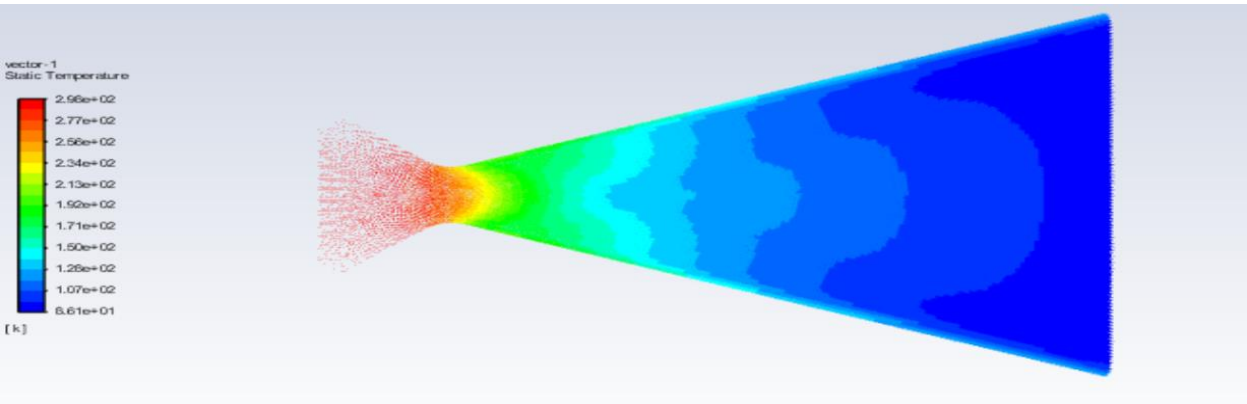

Pressure Contour at 25° Divergence Angle:

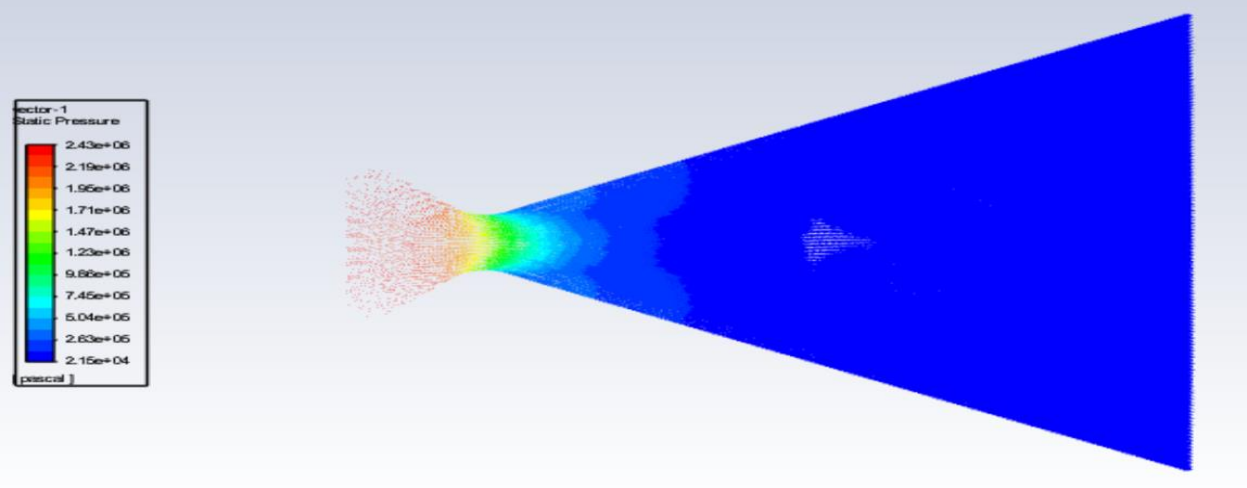

Velocity Contour at 25° Divergence Angle:

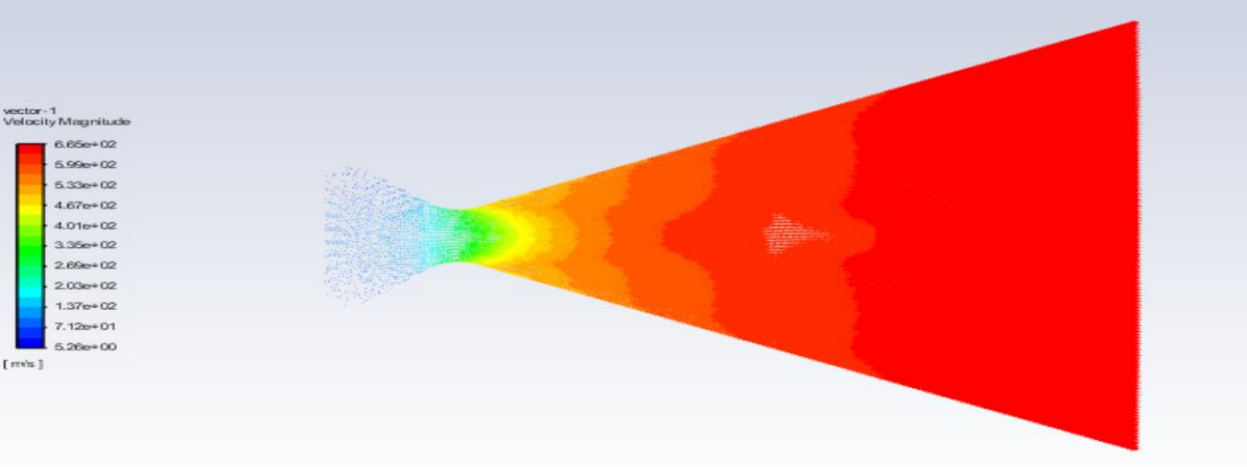

Temperature Contour at 25° Divergence Angle:

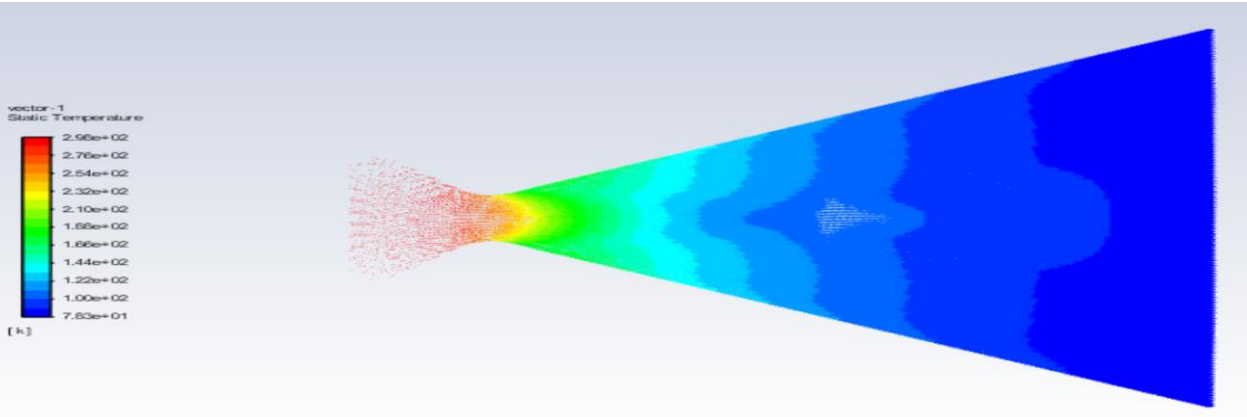

Pressure Contour at 30° Divergence Angle:

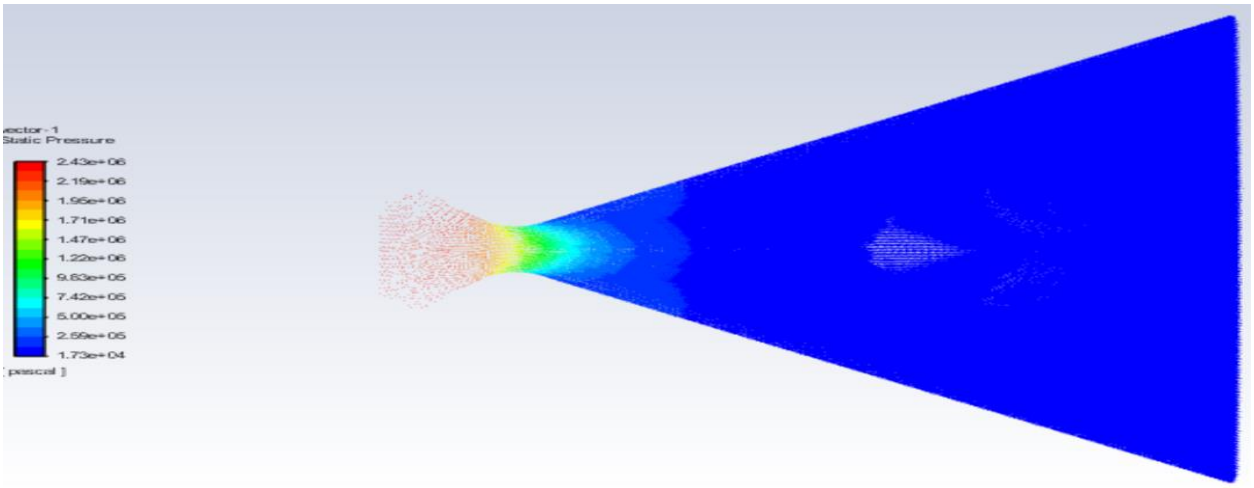

Velocity Contour at 30° Divergence Angle:

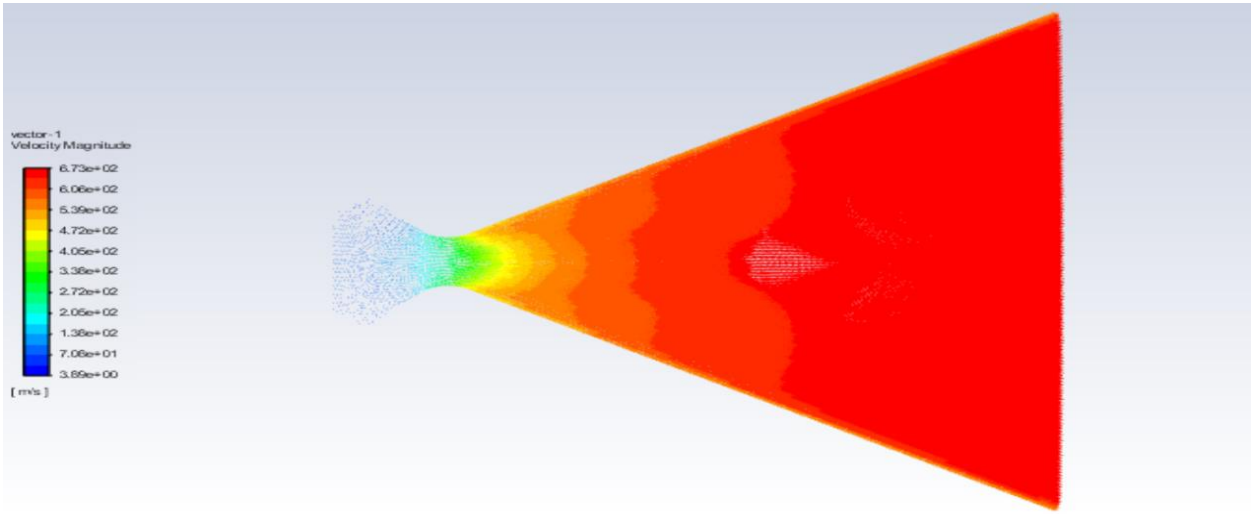

Temperature Contour at 30° Divergence Angle:

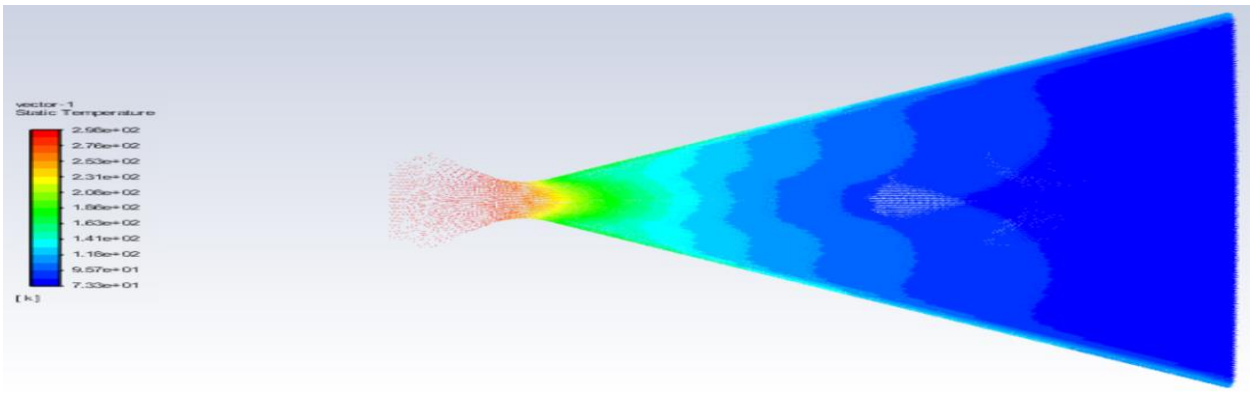

APPENDIX B:

DIVERGENT LENGTH GEOMETRY

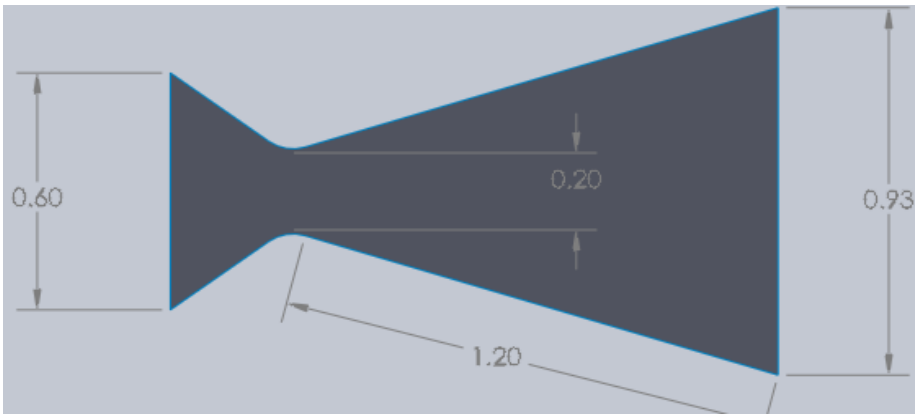

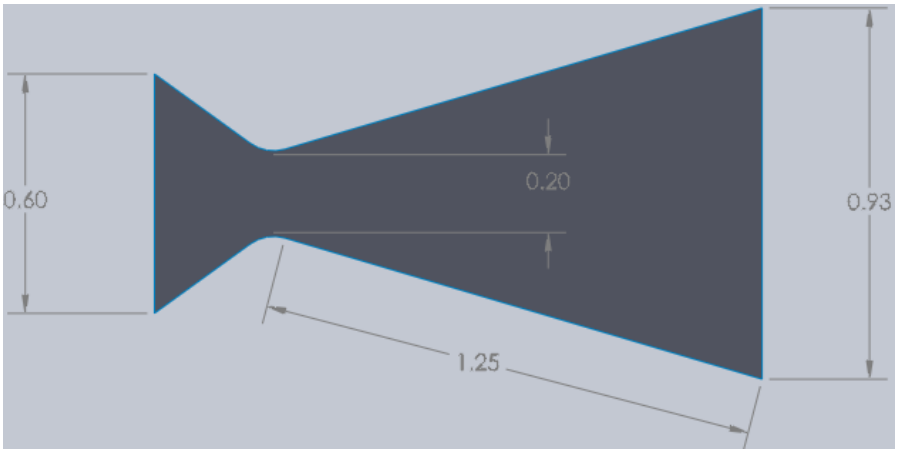

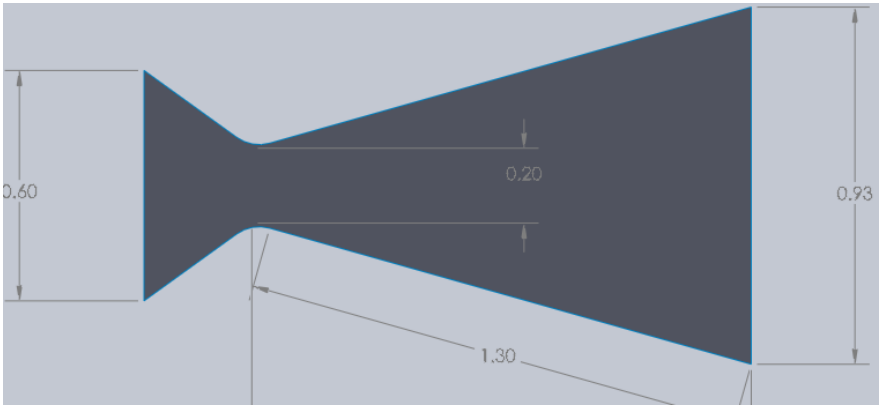

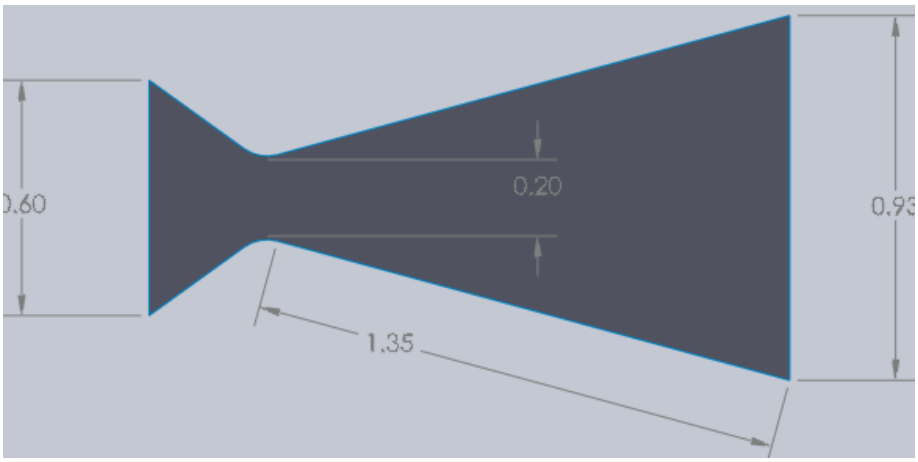
0.60
0.20
0.93
1.35

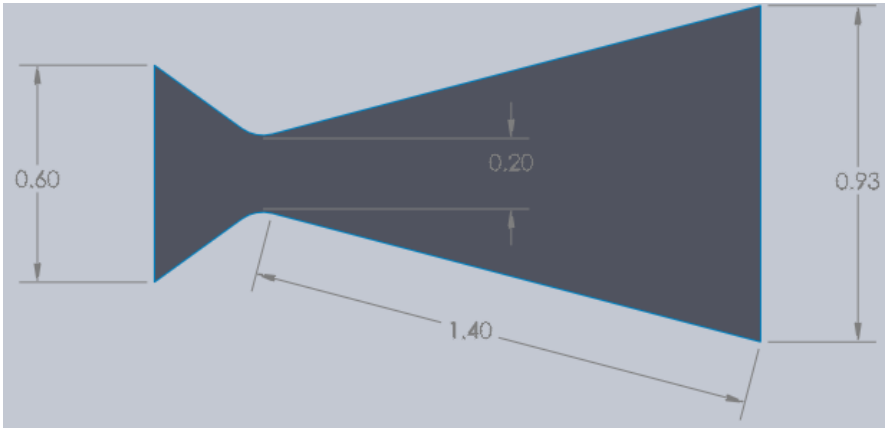
0.60
0.20
0.93
1.40

REFERENCES

3D Printing in Space. (2014). In *3D Printing in Space*. National Academies Press. https://doi.org/10.17226/18871

Ahmer, D. Z., Shah, M. A., Sultan, S., & Shah, S. M. A. (2014). Design Optimization through Numerical Simulations and Testing of 5N Cold Gas Thruster. *Journal of Space Technology*, *4*, 3–10.

Ande, R., & Kumar Yerraboina, V. N. (2018). Numerical investigation on effect of divergent angle in convergent-divergent rocket engine nozzle. *Chemical Engineering Transactions*, *66*(2010), 787–792. https://doi.org/10.3303/CET1866132

Anis, A. (2012). Cold Gas Propulsion System - An Ideal Choice for Remote Sensing Small Satellites. *Remote Sensing - Advanced Techniques and Platforms*. https://doi.org/10.5772/37149

Argyropoulos, C. D., & Markatos, N. C. (2015). Recent advances on the numerical modelling of turbulent flows. *Applied Mathematical Modelling*, *39*(2), 693–732. https://doi.org/10.1016/j.apm.2014.07.001

Aysu, O. (2019). *Performance Characteristics of a Cold Gas Thruster With Real Gas Conditions* (Issue September).

Belega, B.-A., & Duc Nguyen, T. (2015). *"Henri Coanda" "General M.R. Stefanik" Air Force Academy Armed Forces Academy Romania Slovak Republic Analysis of Flow in Convergent-Divergent Rocket Engine Nozzle Using Computational Fluid Dynamics*.

Blog, A. E. (n.d.). *Supersonic Aerodynamics: Designing Rocket NozzlesAerospace Engineering Blog*. Retrieved August 8, 2021, from https://aerospaceengineeringblog.com/supersonic-aerodynamics-designing-rocket-nozzles/

Caughey, D. A. (2004). Computational fluid dynamics. In *Computer Science Handbook, Second Edition*. https://doi.org/10.1017/cbo9780511780066

Celik, I. B. (Wester. V. U. (1999). Introductory turbulence modeling. *Western Virginia University Class Notes*, *December*, 94. http://www.fem.unicamp.br/~im450/palestras&artigos/ASME_Tubulence/cds13workbook.pdf

Corradini, M. L., Zhu, C., Fan, L. S., & Jean, R. H. (2016). Multiphase flow. In *Handbook of Fluid Dynamics: Second Edition*. https://doi.org/10.1201/b19031-24

Croteau, T. (2018). *Micro-Nozzle Simulation and Test for an Electrothermal Plasma Thruster*. *December*.

Denton, B. L., & Denton, B. L. (2008). *Design and analysis of rocket nozzle contours for launching Pico- Satellites Design and Analysis of Rocket Nozzle Contours for Launching Pico-Satellites By*.

Dumitrescu, O., Gherman, B., & Tipa, T. (2018). Development of a Laval nozzle for a cold gas propulsion system. *IOP Conference Series: Materials Science and Engineering*, *400*(4). https://doi.org/10.1088/1757-899X/400/4/042016

FAA. (2017). Advanced Aerospace Medicine On-line Section III Space Operations: Rockets and Launch Vehicles. *Advanced Aerospace Medicine On-Line - Section III - Space Operations*, 506–551. https://www.faa.gov/about/office_org/headquarters_offices/avs/offices/aam/cami/library/online_libraries/aerospace_medicine/tutorial/media/III.4.2.1_Rockets_and_Launch_Vehicles.pdf

Fabiano, A. J., & Qiu, J. (2015). FVM vs FDM. *Journal of Neurosurgical Sciences*, *59*(2), 157–167. http://www.erac.ntut.edu.tw/ezfiles/39/1039/img/832/3-1-00001-intro-FiniteDifference.pdf

Goebel, D. M., & Katz, I. (2008). Fundamentals of Electric Propulsion: Ion and Hall Thrusters. *Fundamentals of Electric Propulsion: Ion and Hall Thrusters*, 1–507. https://doi.org/10.1002/9780470436448

Jahn, R. G., & Lyman, F. A. (1969). Physics of Electric Propulsion. In *Journal of Applied Mechanics* (Vol. 36, Issue 3, pp. 655–655). https://doi.org/10.1115/1.3564751

Jamshed, S. (2015). Introduction to CFD. *Using HPC for Computational Fluid Dynamics*, 1–20. https://doi.org/10.1016/B978-0-12-801567-4.00001-5

Kalsch I. (2000). *Chemical Spacecraft Propulsion in ESA: Current Activities - NASA/ADS*. 41. https://ui.adsabs.harvard.edu/abs/2000ESASP.465...41K/abstract

Kramer, H. J., & Cracknell, A. P. (2008). An overview of small satellites in remote sensing. *International Journal of Remote Sensing*, *29*(15), 4285–4337. https://doi.org/10.1080/01431160801914952

Krejci, D., & Lozano, P. (2018). Space Propulsion Technology for Small Spacecraft. *Proceedings of the IEEE*, *106*(3), 362–378. https://doi.org/10.1109/JPROC.2017.2778747

Kundu, A., Prasad, D., & Ahmed, S. (2007). Effect of Exit Diameter on the Performance of Converging – Diverging Annular Nozzle Using CFD. *International Journal of Innovative Research in Science, Engineering and Technology (An ISO Certified Organization)*, *3297*(6), 9726–9734. https://doi.org/10.15680/IJIRSET.2015.0506031

Length, C. S., Nozzle, S., Engineering, M., & Uet, M. (2017). *Influence od convergent section Length and Angle on Performance of Supersonic Nozzle*. *49*(004), 727–732.

Levchenko, I., Xu, S., Teel, G., Mariotti, D., Walker, M. L. R., & Keidar, M. (2018). Recent progress and perspectives of space electric propulsion systems based on smart nanomaterials. *Nature Communications*, *9*(1). https://doi.org/10.1038/S41467-017-02269-7

Lieu, nguyen thi. (2015). Turbulence Modelling. *Nhk技研*, *151*, 10–17.

Lin, X., Li, X., & Lin, X. (2020). A Review on Applications of Computational Methods. *Molecules*, *25*(6), 1375.

Lule, T. K., & Lule, M. K. (2016). *Short Review on Electric Propulsion System : Ion Thruster Short Review on Electric Propulsion System : Ion Thruster*. *August 2015*, 0–5. https://doi.org/10.13140/2.1.2331.8406

Material, C. T. (2010). *Methodology Introduction to ANSYS FLUENT*. *December*, 1–17.

Murphy, D. M., & Trautt, T. A. (2007). *Solar Sail Propulsion*. *April*, 1–17.

Mzad, H., & Elguerri, M. (2012). Theoretical and Experimental Investigation of Compressible Flow through Convergent–Divergent Nozzles. *Advanced Materials Research*, *452–453*, 1277–1285. https://doi.org/10.4028/SCIENTIFIC5/AMR.452-453.1277

Nikolova, I. (2005). *S e s ' 2 0 0 5*. *June*, 515–518.

Poradowski, W. (n.d.). *Lecture 7: Turbulence Modeling Introduction to ANSYS Fluent*. Retrieved August 13, 2021, from https://www.academia.edu/36090206/Lecture_7_Turbulence_Modeling_Introduction_to_ANSYS_Fluent

Ranjan, R., Karthikeyan, K., Riaz, F., & Chou, S. K. (2018). Cold gas propulsion microthruster for feed gas utilization in micro satellites. *Applied Energy*, *March*, 1–13. https://doi.org/10.1016/j.apenergy.2018.03.040

Roddy, M. A. (2020). *ScholarWorks @ UARK Development of High-Density Propulsion System Technologies for Interplanetary Small Satellites and CubeSats*.

Salgado, M. C. V., Belderrain, M. C. N., & Devezas, T. C. (2018). Space propulsion: A survey study about current and future technologies. *Journal of Aerospace Technology and Management*, *10*, 1–23. https://doi.org/10.5028/jatm.v10.829

Seubert, C. R., Pernicka, H. J., & Norgren, C. L. (2007). Refrigerant-based propulsion system for small spacecraft. *Collection of Technical Papers - 43rd AIAA/ASME/SAE/ASEE Joint Propulsion Conference*, *2*, 1347–1359. https://doi.org/10.2514/6.2007-5131

Singh, J., Zerpa, L. E., Partington, B., & Gamboa, J. (2019). Effect of nozzle geometry on critical-subcritical flow transitions. *Heliyon*, *5*(2), e01273. https://doi.org/10.1016/j.heliyon.2019.e01273

Sutton, G. P., & Biblarz, O. (2010). *Rocket Propulsion Elements*. John Wiley & Sons.

Tan, M. L. S., Alemania, T. A. B., Ong, W. C. J., & Augusto, G. L. (2019). *Microsatellites Using Computational Fluid Dynamics and Response Surface Optimization*. 1–4.

Tummala, A. R., & Dutta, A. (2017). An overview of Cube-Satellite propulsion technologies and trends. *Aerospace*, *4*(4), 1–30. https://doi.org/10.3390/aerospace4040058

Turner, M. J. L. (2008). *Rocket and Spacecraft Propulsion Principles, Practice and New Developments (Second Edition)* (Vol. 2). http://www.pyrobin.com/files/rocket and spacecraft propulsion 3540221905_1.pdf

William J Devenport. (n.d.). *Converging Diverging Nozzle*. Retrieved August 8, 2021, from https://www.engapplets.vt.edu/fluids/CDnozzle/cdinfo.html